

## Pressure effects on the electronic structure and low-temperature states in the $\alpha$ -(BEDT-TTF) $_2$ MHg(SCN) $_4$ organic-conductor family ( $M = \text{K, Rb, Tl, NH}_4$ )

J. S. Brooks\* and X. Chen<sup>†</sup>

*Department of Physics, Boston University, Boston, Massachusetts 02215*

S. J. Klepper

*F. B. National Magnet Laboratory, Massachusetts Institute of Technology, Cambridge, Massachusetts 02139*

S. Valfells and G. J. Athas

*Department of Physics, Boston University, Boston, Massachusetts 02215*

Y. Tanaka, T. Kinoshita, N. Kinoshita, and M. Tokumoto

*Electrotechnical Laboratory Tsukuba, Ibaraki 305, Japan*

H. Anzai

*Himeji Institute of Technology, 2167 Shosya, Himeji, Hyogo 671-22, Japan*

C. C. Agosta

*Physics Department, Clark University, Worcester, Massachusetts 01610*

(Received 30 January 1995; revised manuscript received 28 July 1995)

We have used the magnetoresistance and the Shubnikov-de Haas effect to study the pressure-dependent ground states of  $\alpha$ -(BEDT-TTF) $_2$ MHg(SCN) $_4$  [where BEDT-TTF is alpha-bis(ethylenedithio) tetrathiafulvalene- $M$  ( $=$ potassium, rubidium, thallium, or ammonium)-mercury-thiocyanate]. Extended Hückel tight-binding calculations show that this isostructural class of materials has a quasi-two-dimensional Fermi surface with both open and closed orbit bands. Both superconducting ( $M = \text{NH}_4$ ) and density-wave ( $M = \text{K, Tl, and Rb}$ ) states in these materials have been investigated. We report the effects of pressure on the electronic structure (Fermi surface), the density-wave state, and the superconducting state. We find (where  $M = \text{Tl}$ , for example) that the fundamental closed-orbit and Brillouin-zone areas increase with pressure at a rate of 1.3%/kbar and 0.5%/kbar, respectively. We observe pressure-induced changes in the nesting condition of the open-orbit band that allow new small closed orbits on the Fermi surface. The onset of quasi-three-dimensional behavior with increasing pressure is observed in some cases. In those materials with density-wave states, the associated resistive anomalies are removed between 6 and 8 kbar. In the superconducting member ( $M = \text{NH}_4$ ), pressure decreases the superconducting transition temperature  $T_c$  as  $dT_c/dP \approx -0.25$  K/kbar, with a corresponding reduction in the effective mass. From analysis of the pressure dependence of  $T_c$  we find that the interaction term in the mean-field expression for superconductivity is very sensitive to pressure. We note that the pronounced pressure dependence of the electronic properties of these materials provides fertile ground for future studies of low-dimensional phenomena.

### I. INTRODUCTION

The isostructural family of organic conductors<sup>1-3</sup>  $\alpha$ -(BEDT-TTF) $_2$ MHg(SCN) $_4$  (where BEDT-TTF is alpha-bis(ethylenedithio) tetrathiafulvalence) has been the subject of considerable attention due to the observation of superconductivity<sup>4</sup> in  $\alpha$ -(BEDT-TTF) $_2$ NH $_4$ Hg(SCN) $_4$  and a low-temperature state<sup>5</sup> in  $\alpha$ -(BEDT-TTF) $_2$ MHg(SCN) $_4$  (where  $M = \text{K, Rb, or Tl}$ ). The temperature-magnetic field-pressure phase diagrams of these materials are shown in Fig. 1. The materials, which are charge-transfer salts, have  $\alpha$ -type stacking of the cations in inequivalent adjacent chains, thereby making conducting molecular planes in the  $a$ - $c$  direction. Details of the crystal structure and the resulting band structure and Fermi-surface (FS) topology are shown in Fig. 2. The anion

complex MHg(SCN) $_4$  is particularly thick ( $\approx 7$  Å), thereby causing considerable separation of the cation layers along the  $b$  axis. Hence the conducting cation layers are highly two dimensional in electronic character. Extended Hückel-tight-binding band calculations<sup>6,7</sup> indicate the presence of both closed hole orbits and open electronlike orbits on the Fermi surface.

The title materials are of particular importance due to the interplay of the two-dimensional Fermi surface, which yields the Shubnikov-de Haas effect, and the one-dimensional Fermi surface, which influences the ground state (density-wave-like, or superconducting) of the material. The open orbits are thought to undergo a Peierls-type transition in some cases. The closed orbits remain in their original or in a reconstructed Fermi-surface topology. The result of this interplay is a highly unusual set of anisotropic magnetic-field-dependent properties that are

observed at low temperatures. Attempts to understand this complex behavior involve a mixture of well-established methods of Fermiology<sup>8</sup> and other treatments of angular-dependent magnetotransport in low-dimensional systems.<sup>9</sup> In the case of the traditional methods of Fermiology, even the application of the

Lifshitz-Kosevich formalism<sup>8</sup> (valid for three-dimensional Fermi surfaces) to the highly two-dimensional closed-orbit Fermi surfaces encountered in these materials can be questioned.<sup>10,11</sup> Hence these materials provide a truly rich area for theory and experiment in low-dimensional systems. We will show in this paper that the very large compressibility of the title materials, which is an order of magnitude greater than in common metals, provides a powerful method to study their electronic structure and ground-state properties.

In this paper the terms low-temperature state (LTS) and/or density wave (DW) are used to describe the low-temperature and low-magnetic-field state that is observed for  $M=K, Rb$ , and  $Tl$ , sometimes referred to as the DW salts. The LTS exists below a transition temperature  $T_{DW}$  and below a critical “kink” field  $H_{kink}$ . The nature of the ground state [charge density wave (CDW), vs spin density wave (SDW)] is still a matter of controversy—recent muon spin resonance measurements<sup>12</sup> report a SDW moment of  $0.003\mu_B$ , but <sup>13</sup>C nuclear magnetic resonance measurements<sup>13</sup> have been interpreted as showing no onset of magnetic order. Finally, there is evidence that there may be subphases associated with the LTS,<sup>14,12</sup> and complex behavior at very low temperatures at fields near and above the so-called kink field transition<sup>15</sup> has also been reported.

The present work<sup>16</sup> was motivated by several considerations. The variance of unit-cell volume with anion structure<sup>17</sup> is  $[M, V (\text{\AA}^3)] = [Tl, 1990]$ ,  $[K, 1997]$ ,  $[NH_4, 2010]$ , and  $[Rb, 2020]$ . If the difference between the superconducting and density-wave materials only involved the unit-cell volume, then it might be possible to induce superconductivity for  $M=Rb$  by reducing its unit cell to that of the superconducting member  $M=NH_4$ . Or, the density-wave state associated with  $M=K$  might be induced in  $M=NH_4$  by similar means. A second motivation was to apply pressure to suppress the density-wave state and to compare the results with the known effects of pressure on other materials with low-temperature ground states.

The rest of this paper is organized as follows. In Sec. II we provide a brief review of the most important physical properties of these materials, and in Sec. III the effects of pressure on electronic structure and superconductivity are discussed. Section IV gives the experimental details and a summary of the most important effects of pressure on the properties of the title materials. In Sec. V we present the effects of pressure on each member of the  $\alpha$ -(BEDT-TTF)<sub>2</sub>MHg(SCN)<sub>4</sub> series. Section VI provides a perspective on our findings, and we discuss the results in light of the present understanding of the electronic structure and its effects on the physical properties of these materials. Finally, we review our findings in the concluding Sec. VII.

## II. BRIEF REVIEW OF THE PROPERTIES OF THE $\alpha$ -(BEDT-TTF)<sub>2</sub>MHg(SCN)<sub>4</sub> FAMILY

Before discussing in detail the effects of pressure, we briefly review the salient features of the title materials. Behavior representative of the LTS is shown in Figs. 3

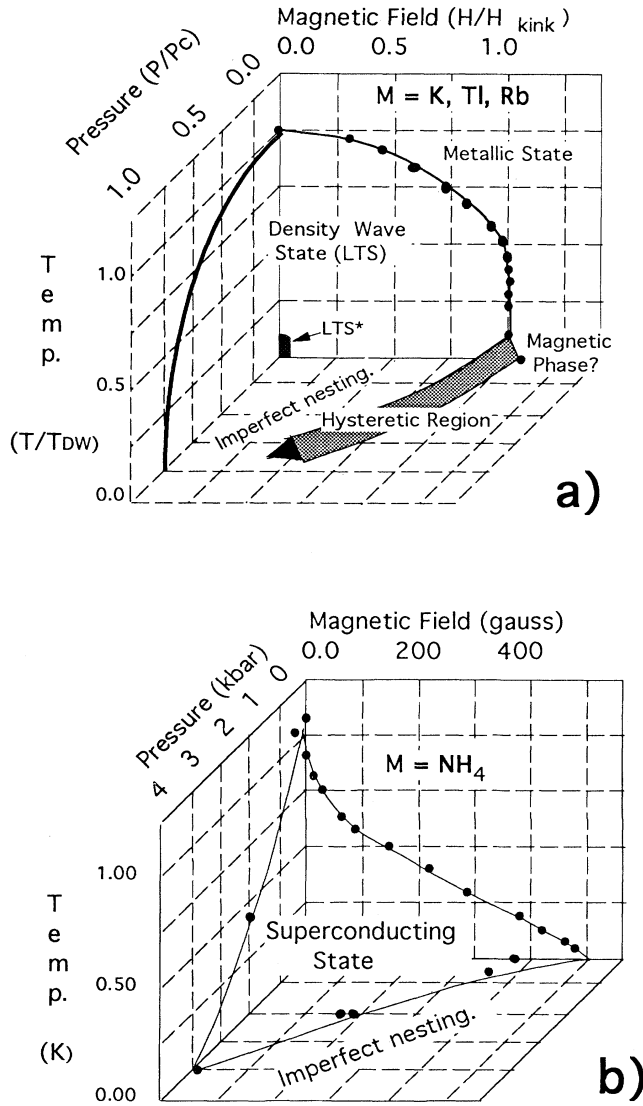


FIG. 1.  $T$ - $H$ - $P$  phase diagram of the  $\alpha$ -(BEDT-TTF)<sub>2</sub>MHg(SCN)<sub>4</sub> materials for  $H\parallel b$  axis. (a) Phase diagram of the DW salts in terms of the reduced parameters  $T/T_{DW}$ ,  $H/H_{kink}$ , and  $P/P_c$ . For  $M=K, Tl$ , and  $Rb$ , respectively:  $T_{DW}=8, 10$ , and  $12$  K;  $H_{kink}=22.5, 23$ , and  $32$  T;  $P_c \approx 4-8$  kbar. Zero-pressure  $T$ - $H$  plane:  $H_{kink}$  (Ref. 27); zero-field  $T$ - $P$  plane (Ref. 17);  $P$ - $H$  plane at low temperatures (this work); LTS\* (Refs. 42 and 44) (size exaggerated for clarity). (b) Phase diagram for the superconductor with  $M=NH_4$ . Zero-pressure  $P$ - $T$  line (Ref. 40); other points (this work).

and 4 for  $M=\text{Rb}$  and  $\text{K}$ , respectively. A resistivity anomaly [see small peak in Fig. 3(a)] appears below a temperature  $T_{\text{DW}}$ , which starts at about 8 K for  $\text{K}$ ,<sup>18</sup> 10 K for  $\text{Tl}$ ,<sup>17</sup> and 12 K for  $\text{Rb}$ .<sup>19</sup> Anisotropic changes in the susceptibility<sup>20–22</sup> and electron spin resonance<sup>23</sup> also occur at these transitions, which have been interpreted as the onset of in-plane antiferromagnetic order. Below the transition temperature, large magnetoresistance is observed [e.g., Figs. 3(b), 4(a), and 4(b)] which becomes negative above a peak field  $H_{\text{max}}$ . At higher fields, a hysteretic anomaly is observed in the magnetoresistance—the so-called “kink field”  $H_{\text{kink}}$  transition, which occurs at about 22.5 T for  $\text{K}$ ,<sup>24</sup> 23 T for  $\text{Tl}$ ,<sup>25,26</sup> and 32 T for  $\text{Rb}$ .<sup>27</sup>

For all of the title materials, quantum oscillations are observed with a fundamental frequency  $F_{\alpha}$ . However, for the DW materials, in addition to  $F_{\alpha}$ , large second and higher harmonic content in the Shubnikov–de Haas (SdH) and de Haas–van Alphen (dHvA) quantum oscillations are observed. The second harmonic effect has been treated as a spin-splitting effect by some authors,<sup>28</sup> in terms of harmonic ratios of the fundamental orbital frequency by others,<sup>29,30</sup> and recently a model involving metallic and DW domains has been suggested.<sup>31</sup> In addition to strong harmonic content in the SdH oscillations, a distinctly different frequency [ $F_{\beta}$  in Fig. 4(c)] at about 4200 T is seen. This is the contribution from the magnetic breakdown between open- and closed-orbit bands, and corresponds to the area of the entire Brillouin zone (BZ).

Within the LTS, unusual angular dependence of the magnetoresistance at constant magnetic field is observed as is shown in Fig. 3(c). The term AMRO (sometimes ADMRO in the literature) refers to the angular-dependent magnetoresistance. In the case of Fig. 3(c), the resistance of the sample is monitored as the angle  $\phi$  between the  $b$  axis of the sample and the direction of the constant applied magnetic field is changed. For temperatures above  $T_{\text{DW}}$ , or fields above  $H_{\text{kink}}$ , the “Yamaji

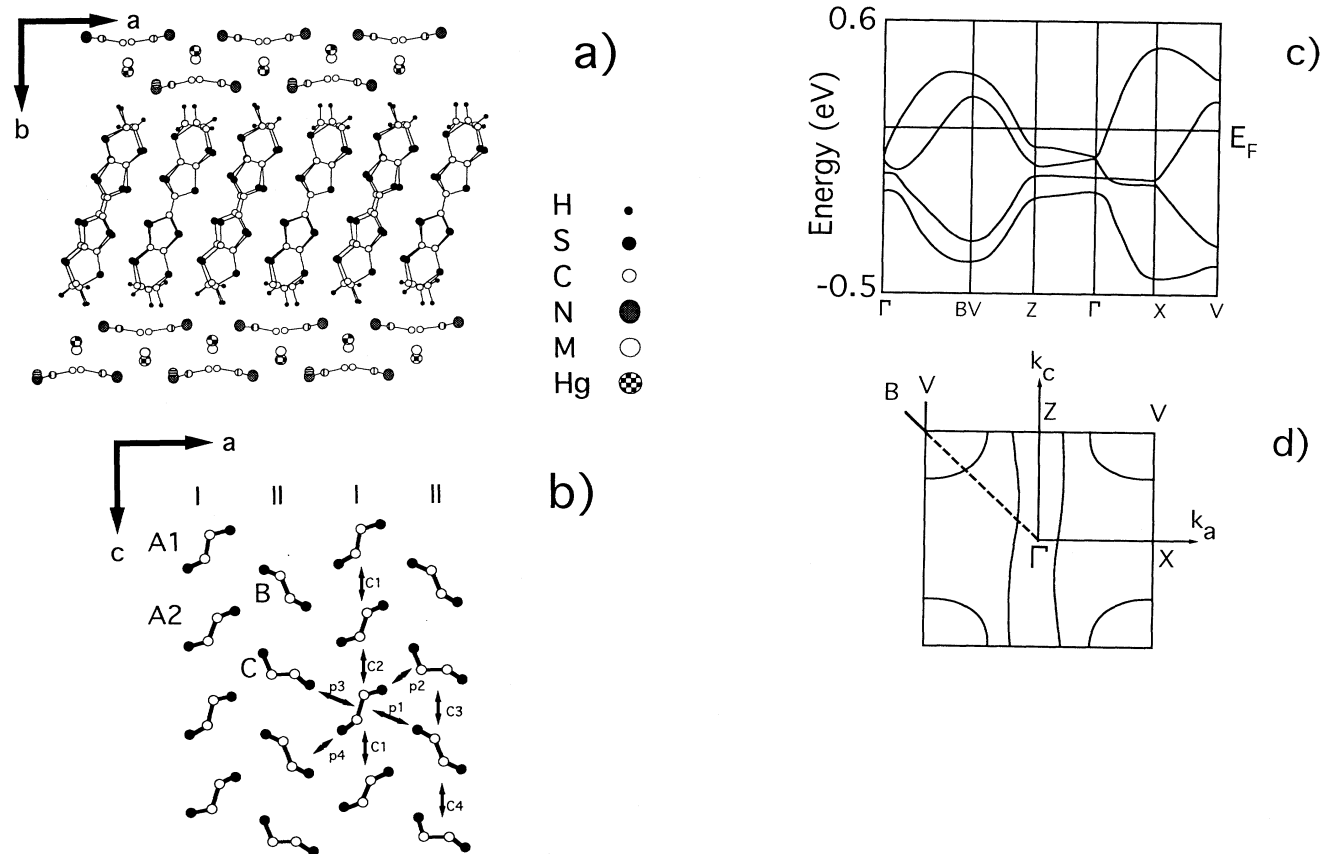


FIG. 2. Physical and electronic structure of  $\alpha$ -(BEDT-TTF)<sub>2</sub>MHg(SCN)<sub>4</sub> (redrawn after Ref. 1) (a)  $a$ - $b$  plane of the  $\alpha$ -(BEDT-TTF)<sub>2</sub>MHg(SCN)<sub>4</sub> molecular crystal structure. The dimensions of the three crystallographic directions for  $M=\text{NH}_4$  (in Å)  $a=10.082$ ;  $b=20.565$ ;  $c=9.933$ . (b)  $a$ - $c$  plane stacking arrangement of donor molecules showing directions of the anisotropic transfer integral terms ( $C$ 's and  $p$ 's) used in the band-structure calculations. I and II refer to the equivalent chains, and A1, A2, B, and C refer to the four different BEDT-TTF sites. (c) Extended Hückel–tight-binding band structure. The four bands are a result of the four inequivalent BEDT-TTF cation sites in the unit cell. (d) Fermi surface with open ( $\Gamma$  center) and closed ( $V$  center) orbits.

effect” behavior<sup>32</sup> is observed. Here peaks are observed in the magnetoresistance that are periodic in  $\tan(\phi)$ , a characteristic of a warped, cylindrical [quasi-two-dimensional (Q2D)] Fermi surface. Below  $T_{DW}$  and  $H_{kink}$ , i.e., within the LTS, a new effect is observed that exhibits dips in the AMRO. These are also periodic in  $\tan(\phi)$ , but the period is highly dependent on the axis of rotation in the  $a$ - $c$  plane. This new behavior has been reported by Kagoshima *et al.*<sup>33</sup> and Caulfield *et al.*<sup>34</sup> for  $M=K$ , by Kartsovnik *et al.*<sup>25</sup> for  $M=Ti$  and Rb, and by Athas *et al.*<sup>35</sup> for  $M=Rb$ . The behavior is relevant to this paper, since it is from such measurements that the

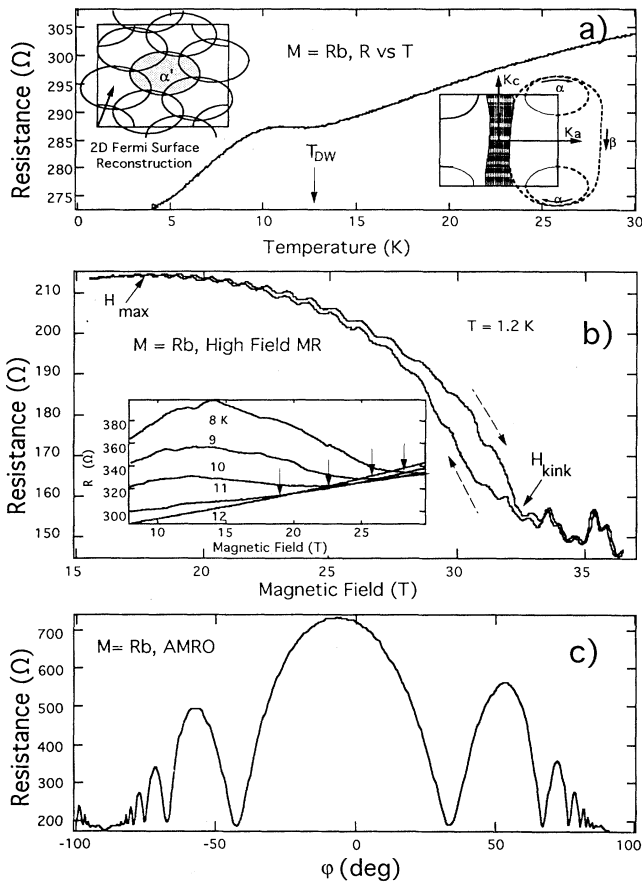


FIG. 3. Ambient pressure transport properties of  $\alpha$ -(BEDT-TTF)<sub>2</sub>RbHg(SCN)<sub>4</sub>. The current is parallel to the  $b$  axis in all cases. (a) Resistive anomaly at  $T_{DW}$ . As shown, the Fermi surface is expected to be metallic above  $T_{DW}$  and reconstructed at lower temperatures. The hole orbit  $\alpha$  and the magnetic breakdown orbit  $\beta$  are possible in the metallic state. In the reconstructed state the hole orbit (here shown as  $\alpha'$ ) is nested (arrow represents the nesting vector), and becomes a magnetic breakdown orbit. (b) High-magnetic-field magnetoresistance showing the resistance maximum at magnetic field  $H_{max}$ , the “kink field”  $H_{kink}$ , and hysteretic behavior for up and down magnetic field sweeps just below  $H_{kink}$ . The inset shows the behavior of  $H_{kink}$  (arrows) at higher temperatures. (c) Angular-dependent magnetoresistance within the LTS.  $\phi$  is the angle between the magnetic field (12 T) and the  $b$  axis—the dip positions are periodic in  $\tan(\phi)$ .

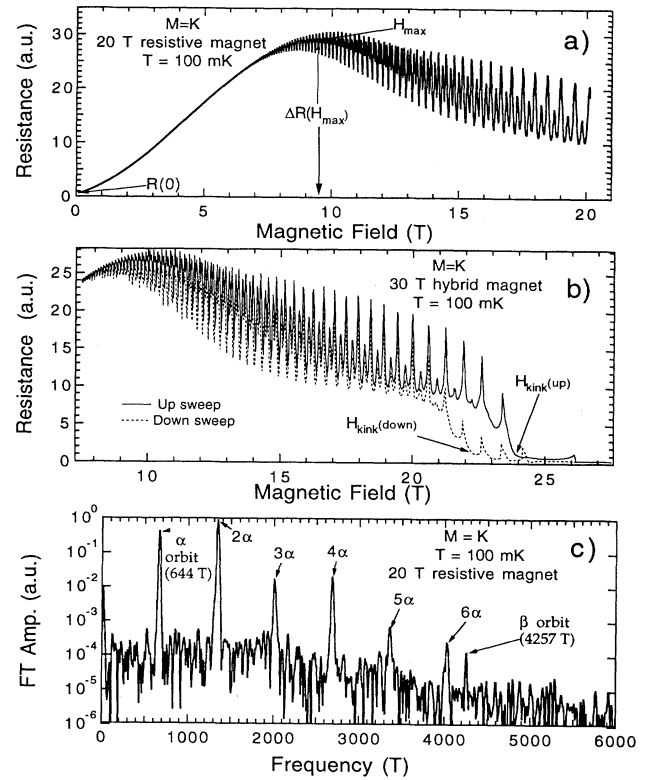


FIG. 4. Magnetoresistance and Shubnikov–de Haas oscillations in  $\alpha$ -(BEDT-TTF)<sub>2</sub>KHg(SCN)<sub>4</sub>. (a) Between 0 and 20 T. (See text for discussion of terms.) (b) Between 7 and 28 T. (c) FT spectrum showing large second and higher harmonic amplitudes for the  $\alpha$  orbit and the presence of the magnetic breakdown orbit  $\beta$ .

Fermi-surface topology of the LTS is deduced. Several authors have proposed that a Fermi-surface reconstruction may exist within the LTS due to a Peierls-like transition.<sup>36,34</sup> [A likely form for this reconstruction is sketched in Fig. 3(a)]. In recent measurements the magnetic breakdown orbit  $\beta$  has been observed, which involves tunneling between the closed and open sections of the Fermi surface for  $M=K$  and  $Tl$ , by a field modulation technique,<sup>37,38</sup> and by nonmodulated dc fields for  $M=K$ ,  $Tl$ , and Rb by the present authors. Furthermore, as many as 10 oscillation frequencies have been observed in the range 2–16 T, some of which are temperature dependent.<sup>38</sup> These observations place stringent limits on the nature of the Fermi-surface topology in the LTS. Models in terms of an open orbit commensurability effect<sup>9</sup> and also as a magnetic breakdown effect<sup>39,31</sup> have been put forward to explain the background and oscillatory dip behavior in the AMRO effect.

The only material in the isostructural family that is a bulk superconductor at ambient pressure is  $M=NH_4$  with a  $T_c$  of about 1 K.<sup>4</sup> It is now known that the critical field is highly anisotropic, in line with the behavior expected for a layered, 2D superconductor.<sup>40</sup> It is clear in the case of the 10.4-K superconductor  $\kappa$ -(BEDT-TTF)<sub>2</sub>Cu(NCS)<sub>2</sub> that pressure very rapidly decreases

both  $T_c$  and the effective mass<sup>41</sup> and as we will show this is also true for  $\text{NH}_4$ .

In  $M=\text{K}$ ,<sup>42</sup>  $\text{Tl}$ ,<sup>43</sup> and  $\text{Rb}$ ,<sup>44,43</sup> a further resistance anomaly is observed well below the  $T_{\text{DW}}$  transition. Here the resistance again decreases. This occurs at about 300 mK for  $M=\text{K}$ , and below about 1 K for  $M=\text{Rb}$ . Ito, Kaneko, and Ishiguro have suggested that the effect is due to an interplay between superconductivity and sheet resistance effects.<sup>42</sup> Although the resistance does not approach zero, it does show critical field and current effects. Shielding fractions of less than 1% have been reported, and antiweak localization has also been proposed to describe this behavior.<sup>44</sup> [Some aspects of this behavior are shown in the inset of Fig. 7(a).]

The pressure dependence of the magnetoresistance for  $\alpha\text{-(BEDT-TTF)}_2\text{KHg(SCN)}_4$  is shown in Fig. 5. Here the transport anomalies associated with the LTS are gone by 8 kbar. From temperature, pressure, and field studies of the transport behavior in the DW materials, we have con-

structed a general  $T$ - $P$ - $H$  phase diagram for the LTS as shown in Fig. 1(a). We note that  $T_{\text{DW}}$ ,  $H_{\text{kink}}$ , and  $H_{\text{max}}$  increase monotonically with unit-cell volume for the DW salts. Pressure effects have been investigated in several of these materials by other workers. Of note is the work on  $\alpha\text{-(BEDT-TTF)}_2\text{TIHg(SCN)}_4$  where the temperature dependence of the zero-field resistivity anomaly has been studied as a function of pressure.<sup>17</sup> Their results indicate that the LTS transition temperature (as indicated by the resistive anomaly) is reduced to zero with increasing pressure. Magnetotransport has also been studied in  $\alpha\text{-(BEDT-TTF)}_2\text{KHg(SCN)}_4$  under pressure<sup>45</sup> to map out the temperature–magnetic field–pressure phase diagram with the kink field as the defining parameter for the phase line of the LTS. Finally, the pressure dependence of the AMRO behavior has been studied<sup>46,47</sup>—here the diplane behavior in the AMRO is observed below  $P_c$ , and the peaklike behavior in the AMRO is observed above  $P_c$ . Hence pressure destroys the anomalous AMRO behavior characteristic of the reconstructed FS in the LTS, and restores the original FS with isolated cylindrical closed orbits.

### III. EFFECTS OF PRESSURE ON TIGHT-BINDING AND SUPERCONDUCTING PARAMETERS

The most visible experimental result of the application of hydrostatic pressure to the *electronic structure* of the title materials is that the fundamental closed hole orbit SdH frequency  $F_\alpha$  increases with increasing pressure as shown in Fig. 5. This means that in the simplifying case of a parabolic energy band, the extremal area of the hole orbit at the Fermi level must increase with pressure. The physical effect of hydrostatic pressure is to reduce the lattice constant  $a$ . (Typical numbers for the linear compressibility of organic charge-transfer materials<sup>48</sup> range from about 1 to  $-4 \times 10^{-3}/\text{kbar}$  for different axes, and the volume compressibility is about  $-1 \times 10^{-2}/\text{kbar}$ .) For the free-electron-gas model, we note that independent of dimensionality, the Fermi level, Fermi momentum, and density of states depend on  $a$  as  $E_F \approx 1/a^2$ ,  $k_F \approx 1/a$ , and  $N(E_F=0) \approx a^2$ , respectively. The band mass  $m_b$  is not a function of density. However, the quantity  $d \log N(0)/d \log V = 2, 1$  and  $2/3$  for one-, two-, and three-dimensional systems, respectively. For the nearly free-electron gas, the only new feature is the inclusion of gaps at the BZ boundary. In this picture, the energy dispersion relation is unchanged, and remains parabolic at all pressures since the effective mass of the electron gas does not change with pressure. For the tight-binding model (TBM), used quite successfully to describe the most important features of the electronic structure of organic conductors,<sup>49</sup> we can make more specific predictions about the pressure dependence. If we consider the simple result for a one-dimensional band, then the band energy  $E_\mu$  is given by

$$E_\mu = \epsilon_\mu + \Delta\epsilon_\mu + 4t_a \cos(k_x a) .$$

Here  $\epsilon_\mu$  and  $\Delta\epsilon_\mu$  are the corresponding atomic orbital energy level and its correction in crystal potential, and  $t_a$

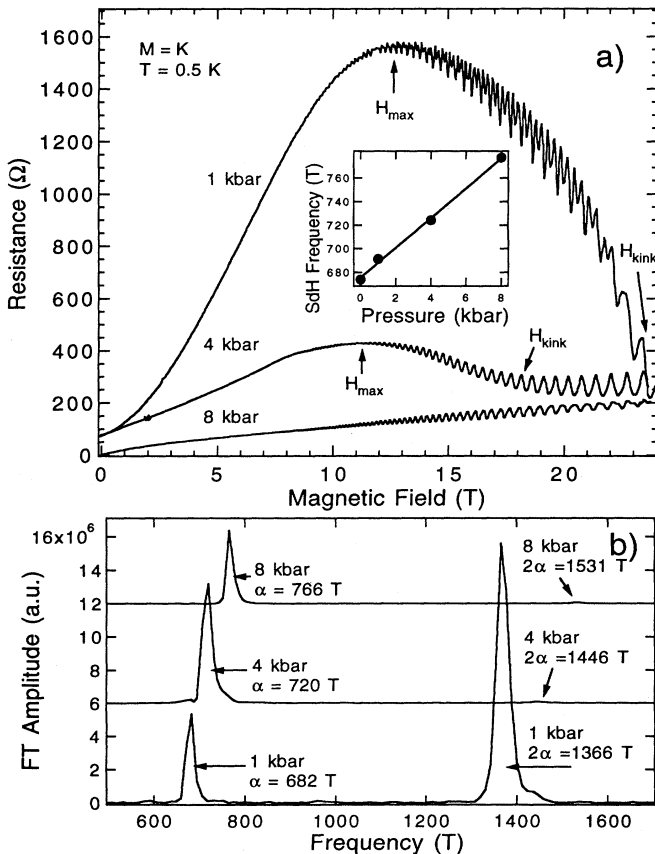


FIG. 5. Pressure dependence of the magnetoresistance of  $\alpha\text{-(BEDT-TTF)}_2\text{KHg(SCN)}_4$  at low temperatures. (a) Magnetoresistance and SdH oscillation behavior vs pressure.  $H_{\text{max}}$  and  $H_{\text{kink}}$  are indicated by arrows. At the lowest pressure the higher harmonic structure in the oscillations is evident. The 8-kbar trace is offset for clarity. The inset shows the change in the fundamental frequency with pressure. (b) Pressure dependence of the Fourier spectrum of the oscillations.

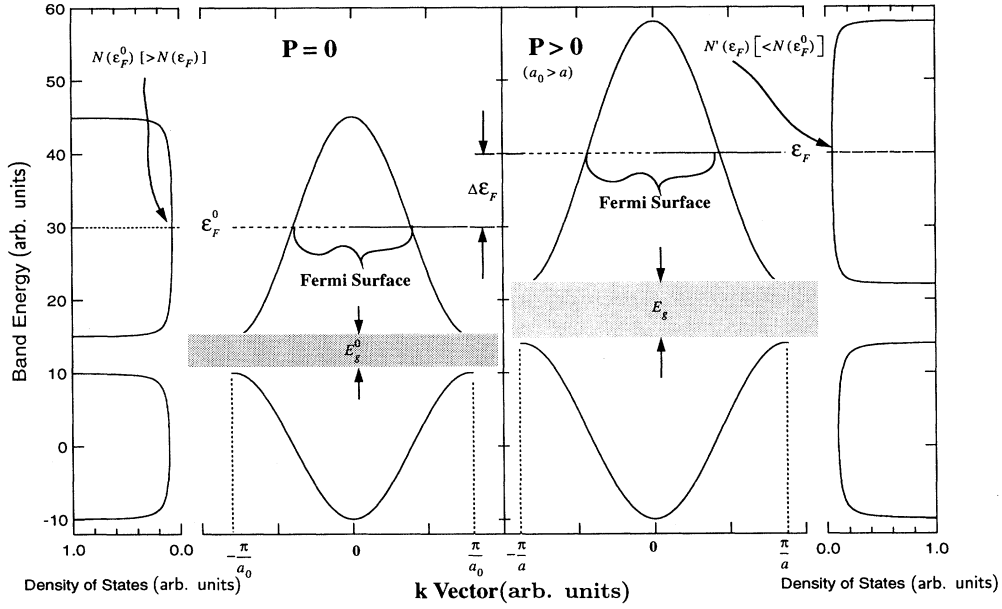


FIG. 6. Schematic pressure dependence of the tight-binding energy band, the Fermi level, and the density of states. On the left, we show the configuration at ambient pressure with lattice constant  $a_0$ , Fermi level  $\epsilon_F^0$ , and band gap  $E_g^0$ . The intersection of the Fermi level and the hole band forms the Fermi surface. On the right, we show the changes that result from a decrease in the lattice constant to  $a$  for increasing pressure: (i) The energy band expands in  $k$  space as the first BZ expands. (ii) The bandwidth increases in energy. (iii) While maintaining the filling of the band, the Fermi level increases by  $\Delta\epsilon_F$ . (iv) The band gap increases to  $E_g$ . (v) The density of states function  $N(\epsilon)$  changes into  $N'(\epsilon)$  (i.e., the density of states at the Fermi level decreases). (vi) The intersection of the band with the Fermi surface increases, which, if extended to two dimensions, means that the associated hole orbit area increases with pressure.

and  $k_x$  are the usual tight-binding bandwidth and momentum, respectively. The effects of pressure on the tight-binding band are shown in Fig. 6. (See also Fig. 19.) Here there are several effects when pressure is increased (i.e., the lattice constant is decreased): (1) The Fermi level  $E_F$  moves up in proportion to  $1/a^2$ , and  $k_F$  increases in proportion to the expansion of the first BZ as  $1/a$ . (2) Electron states become less densely populated both in  $k$  space and in energy as indicated since the electron states are distributed over a wide energy range. Consequently, the density of states at the Fermi level drops. (3) The gap  $E_g$  at the BZ boundary and the bandwidth  $t_a$  increases. Simple estimates of the highly nonlinear pressure dependence of  $t_a$  based on the compressibility and the band-structure parameters<sup>2</sup> suggest that changes of the order 1–100 meV/kbar are possible—that is  $t_a$  can change by as much as the ambient pressure bandwidth. (4) The Fermi-surface topology changes accordingly. The Fermi level is determined by the charge transfer, and the band filling must remain the same at all pressures. Here it is clear that a change in pressure will affect the size of the

hole or electron orbit at the Fermi level. Furthermore, it can be shown<sup>16</sup> that the TBM band mass is relatively insensitive to changes in the lattice constant (i.e., pressure).

Another important effect is the relative change of multiple energy bands with pressure. As we will see, it is possible that the pressure dependence of two bands may differ due to anisotropy in the effects of pressure on the transfer energies.<sup>50</sup> Hence the momentum spacing  $k_t$  between the bands at the Fermi level may change with pressure in a nonmonotonic manner. As shown below, this effect can be measured when magnetic breakdown (interband tunneling of carriers in a magnetic field) is observable.

Finally, we turn to the effects of pressure on superconductivity. As mentioned above, the density of states at the Fermi level will decrease with increasing pressure, which should in principle lower the superconducting transition temperature. One way to approach the problem is in terms of the pressure dependence of the superconducting transition temperature  $T_c$  in terms of the mean-field (BCS) parameters:<sup>16</sup>

$$(-1/\beta T_c)dT_c/dP = -\gamma_g + [1/N(0)V_{\text{BCS}}][d \log N(0)/d \log V + d \log V_{\text{BCS}}/d \log V]$$

where the relation  $\Delta V/V = -\beta\Delta P$  is used to rewrite the right-hand side. Here  $\beta$  is the volume compressibility, and  $\gamma_G$  is the Gruneisen constant. We will show in Sec. VIF that for reasonable estimates of the experimentally accessible terms in the above expression, we may gain information on the pressure dependence of the interaction term  $V_{\text{BCS}}$ .

Another way of looking at the problem is by examination of the effective mass  $m^*$  as determined from the temperature dependence of the SdH amplitude. In principle, this mass is the product of the band mass  $m_b$  and both the electron-phonon interactions  $\lambda_{e-p}$  and electron-electron interactions  $\lambda_{e-e}$ :  $m^* = m_b(1 + \lambda_{e-p})(1 + \lambda_{e-e})$ . Hence the pressure dependence of the effective mass, when compared with the virtually pressure-independent band mass behavior can yield a measure of the pressure dependence of the interaction terms. Recently workers<sup>41,51</sup> have compared measurements of the effective mass by both cyclotron resonance and the SdH effect to discriminate between the electron-phonon and electron-electron terms. Here it is expected that, whereas SdH involves all mass enhancement terms, cyclotron resonance is insensitive to the  $\lambda_{e-e}$  term.

#### IV. EXPERIMENT AND MAIN RESULTS

Samples of  $\alpha$ -(BEDT-TTF)<sub>2</sub>MHg(SCN)<sub>4</sub> ( $M = \text{NH}_4$ , K, Rb, and Tl) were grown at the Electrotechnical Laboratory in Tsukuba by standard electrochemical methods. Resistivity ratios  $R_{300\text{K}}/R_{4.2\text{K}}$  were generally about 100. Gold leads were attached to the samples in a four-terminal arrangement with gold paint, and placed in a standard beryllium copper pressure clamp.<sup>52</sup> In all cases the current, voltage, and applied magnetic field were along the  $b$  axis of the sample. Measurement currents were generally between 1 and 100  $\mu\text{A}$ . Corrections for differences in pressure between room and low temperatures were made according to standard procedure.<sup>53</sup> Measurements were carried out at the Francis Bitter National Magnet Laboratory in 20-T Bitter and in 30- and 37-T Hybrid magnets, and at the National High Magnetic Field Laboratory in a 20-T superconducting magnet. Standard ac resistance measurements were employed.

Figures 4 and 5 serve to define the terms used in the following sections. The anomalous (“giant”) magnetoresistance in the DW salts is characterized by  $\Delta R = R(H_{\text{max}}) - R(0)$ . Here  $R(H_{\text{max}})$  is the resistance at field  $H_{\text{max}}$  where the maximum resistance is reached and  $R(0)$  is the zero-field resistance. In some cases the ratio  $\Delta R/R(0)$  is also referred to. The field at which the magnetoresistance shows a drastic decrease, and where there is the most hysteresis in the field sweeps is referred to as the “kink field”  $H_{\text{kink}}$ . The frequencies of the observed Shubnikov–de Haas oscillations are determined by standard fast Fourier transform (FT) analysis. Here  $F_\alpha$  and/or  $\alpha$ ,  $2\alpha$ , etc. correspond to the fundamental closed orbit and/or the frequency and the higher harmonics.  $F_\beta$  and/or  $\beta$ ,  $2\beta$ , etc. refer to the magnetic breakdown orbit and/or frequency involving the entire first BZ, and the higher harmonics. For very low-

frequency oscillations where the FT method is unusable, the frequency is determined by the slope of the oscillation peak index vs inverse magnetic field. Fractional changes in the extremal areas  $S(P)$  (in momentum space) of the closed orbits with pressure are expressed as  $d \ln[S(P)]/dP$ .

Of special note is the ratio  $F_\alpha/F_\beta$ , which corresponds to the fractional area of the first BZ taken up by the closed-orbit extremal area. In all of the title materials we have been able to measure both frequencies for a single sample at one temperature and in one sweep of the magnetic field. Both frequencies are known to vary as  $1/\cos(\phi)$ , where  $\phi$  is the angle between the magnetic field and the  $b$  axis. Hence errors can occur in the absolute value of any one frequency measured due to the difficulty in achieving perfect alignment of the sample such that the conducting  $a$ - $c$  plane is normal to the magnetic field. Due to the irregular shape of the tiny crystals studied, we have found that without the ability to rotate the sample *in situ* to determine the lowest value of, for instance,  $F_\alpha$ , misalignments of up to  $20^\circ$  can occur, especially in the confining geometry of a pressure cell. However, since the angular dependence cancels in the ratio  $F_\alpha/F_\beta$ , we may accurately determine the percentage area of the  $F_\alpha$  with respect to the BZ.

The effective mass  $m^*$  and Dingle temperature are a result of the usual  $L$ - $K$  analysis of the temperature dependence of the oscillation amplitudes. It is important to note that we did not consider changes in the magnitude of the background magnetoresistance in the present analysis for the effective mass, nor has the field dependence of the effective mass parameter<sup>10</sup> in the  $L$ - $K$  analysis been taken into account. In cases where the background resistance changes significantly with temperature, this can alter the values of  $m^*$  obtained from the  $L$ - $K$  analysis. Hence the values of  $m^*$  that we quote have some uncertainty, and may be less by  $0.2m_0$ – $0.5m_0$  from values obtained by other methods. Nevertheless, in the case for  $M = \text{NH}_4$ , which does not have a strong temperature dependence in the background magnetoresistance, the pressure dependence of  $m^*$  between 0 and 4 kbar was significantly above our estimated experimental errors. Above 4 kbar,  $m^*$  for  $M = \text{NH}_4$  approached that of the DW salts, and no longer changed with increasing pressure. For the case of the DW salts, we found no systematic dependence of  $m^*$  on pressure.

The work reported here represents a systematic study of the pressure dependence of the magnetotransport and Fermi-surface properties of the  $\alpha$ -(BEDT-TTF)<sub>2</sub>MHg(SCN)<sub>4</sub> family. Some of our original expectations about the pressure effects were realized and many additional findings were obtained. The main effects of pressure the  $\alpha$ -(BEDT-TTF)<sub>2</sub>MHg(SCN)<sub>4</sub> materials, as observed in this work and by previous workers, are as follows.

##### A. Electronic structure

Topological entities on the Fermi surface change with pressure as the energy bands and Fermi level change. These include: (1) the BZ expands with increasing pres-

sure. (2) Closed orbits increase in size. (3) The nesting condition of open orbits (and therefore the existence of small pockets) is believed to change with pressure. (4) The tunneling probability between closed- and open-orbit bands does not seem to increase monotonically with increasing pressure. (5) The effective mass in the DW salts is roughly pressure independent. (6) Pressure increases the 3D character of materials as evidenced by the corresponding onset of beats in the quantum oscillations.

### B. Density-wave behavior

Pressure removes the magnetotransport anomalies associated with the low-temperature–low-magnetic-field density-wave state. For pressures above a critical pressure  $P_c$ : (1) The zero-magnetic-field resistive anomaly<sup>17</sup> transition temperature  $T_{DW}$  goes to zero. (2) The giant magnetoresistance is suppressed from a superlinear to a sublinear power-law dependence on magnetic field. (3) The large second harmonic amplitude of the fundamental quantum oscillation frequency is reduced. (4) The magnetic field at which the magnetoresistance drops dramatically (kink field  $H_{\text{kink}}$ ) decreases. (5) The angular-dependent magnetoresistance characteristic of the LTS (minima in the magnetoresistance) changes to that characteristic of the metallic state (maxima in the magnetoresistance).<sup>46,47</sup>

### C. Superconductivity

In the one member of the title materials that exhibits bulk superconductivity ( $M=\text{NH}_4$ ), pressure rapidly (1) reduces  $T_c$ , (2) reduces the effective mass  $m^*$ , and (3) reduces the normal-state magnetoresistance. Items 1 and 2 suggest a strong dependence of the BCS interaction on pressure. However, we found no evidence to support hydrostatic pressure-induced superconductivity in the DW salts.<sup>54</sup>

## V. PRESSURE-DEPENDENT STUDIES FOR $M=\text{Rb}$ , K, Tl, AND $\text{NH}_4$

### A. Pressure studies of $\alpha\text{-(BEDT-TTF)}_2\text{RbHg(SCN)}_4$

One of the original motivations for the pressure work was to see if superconductivity in the density-wave materials could be induced with pressure. Inspection of the relative unit-cell volumes  $V$  (Ref. 17) shows that  $\alpha\text{-(BEDT-TTF)}_2\text{RbHg(SCN)}_4$  (i.e.,  $M=\text{Rb}$ ) has a larger unit cell of  $2020 \text{ \AA}^3$  than  $\alpha\text{-(BEDT-TTF)}_2\text{NH}_4\text{Hg(SCN)}_4$  (i.e.,  $M=\text{NH}_4$ ), the superconducting member with a value of  $2010 \text{ \AA}^3$ .  $dV/dP$  is of order  $10 \text{ \AA}^3/\text{kbar}$ . Hence we anticipated the possibility that the Rb material would undergo a transition to a superconducting state by 1 kbar, since the  $M=\text{Rb}$  sample should have the same unit-cell volume as the  $M=\text{NH}_4$ . However, our pressure studies revealed no evidence for such an effect.

Many of the ambient pressure properties for  $M=\text{Rb}$  are shown in Fig. 3, and also in Fig. 7. In Fig. 7(a) we show the ambient pressure magnetoresistance (MR) and SdH oscillations for  $M=\text{Rb}$  at very low temperatures in a

20-T superconducting magnet. Of note in the insets are the appearance of the second harmonic in the SdH oscillations, and the magnetic field dependence of the resistance at very low fields (i.e., the LTS\* behavior). In Fig. 7(b) we show the FT analysis, where many harmonics of the fundamental SdH frequency are evident. These data also exhibit the magnetic breakdown orbit  $\beta$ . Here the value of 4234 T represents an extremal area equal to the first BZ. Values of  $F_\beta \approx 4200 \text{ T}$  are observed in all of the materials studied at ambient pressure due to their isostructural nature. The kink field for Rb is the largest of the DW series, of order 32 T. Ambient pressure measurements to 37 T in the new Hybrid III magnet at the F. B. National Magnet Laboratory, where holmium pole pieces were employed to achieve the highest fields possible, are shown in Fig. 3(b). Here the second harmonic is seen in the SdH oscillations, there is a magnetoresistance maximum at the field  $H_{\text{max}}$  near 10 T, and strong hysteretic behavior associated with the kink field  $H_{\text{kink}}$  is ob-

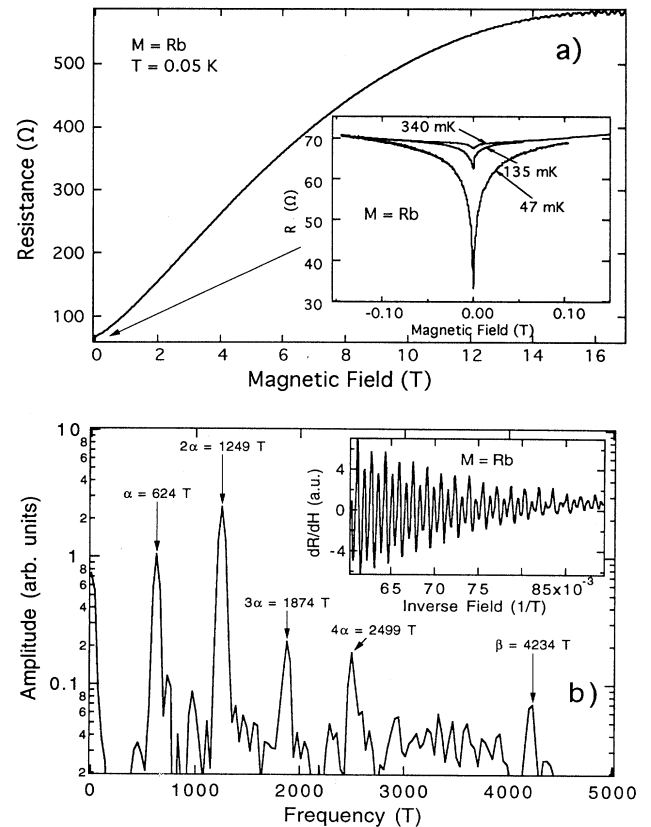


FIG. 7. (a) Ambient pressure magnetoresistance and SdH oscillation of  $\alpha\text{-(BEDT-TTF)}_2\text{RbHg(SCN)}_4$  measured in a 20-T superconducting magnet at 0.05 K. Inset: the temperature dependence and low-field magnetoresistance between  $T_c^*$  ( $< 1 \text{ K}$ ), the range of the LTS\* state. (b) Details of the SdH oscillations [derivative of the resistance with field ( $dR/dH$ ) vs inverse field]. Inset: FT of the  $M=\text{Rb}$  SdH signal showing large second harmonic behavior ( $2\alpha$ ) and also the magnetic breakdown orbit  $\beta$ .

served. The inset shows the behavior of the magnetoresistance at higher temperatures, where the kink field is accessible below 24 T. The fundamental hole orbit frequency is  $F_\alpha = 624$  T at 0 kbar, and from the ratio  $F_\alpha/F_\beta$  we find that the  $\alpha$  orbit corresponds to an extremal area of 15% of the BZ.

The pressure dependence of the MR and SdH effects is shown in Figs. 8(a), 8(b), and 8(c). In Fig. 8(a), we ob-

serve the general trend with pressure, which is to reduce the  $\Delta R$  value with increasing pressure. We also note that  $M=Rb$  seems to have the lowest quality SdH oscillations, at least at ambient pressure, of the entire family, although the AMRO oscillations [see Fig. 3(c)] can be quite sharp. Under pressure the oscillation amplitude increases, and the second harmonic is eventually suppressed by 4 kbar. For higher pressures, the kink field

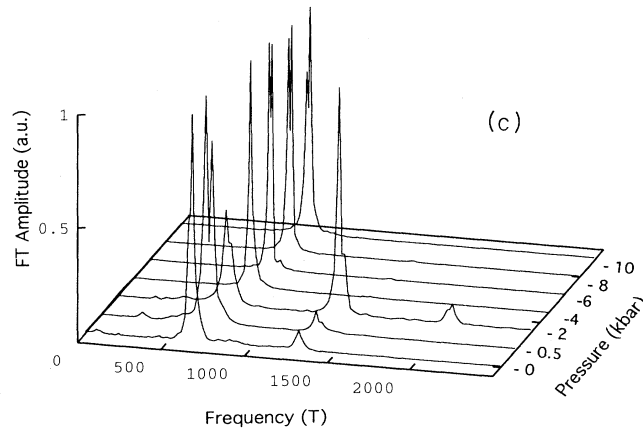
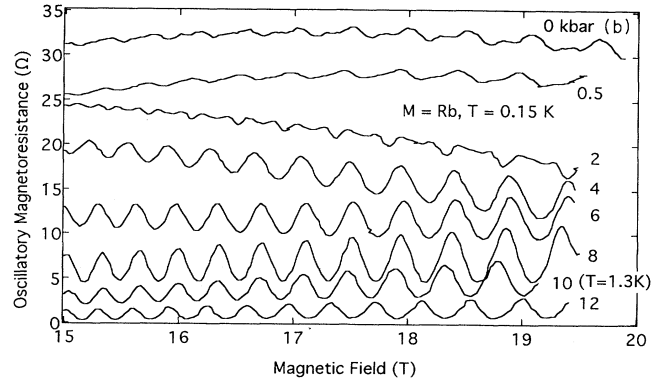
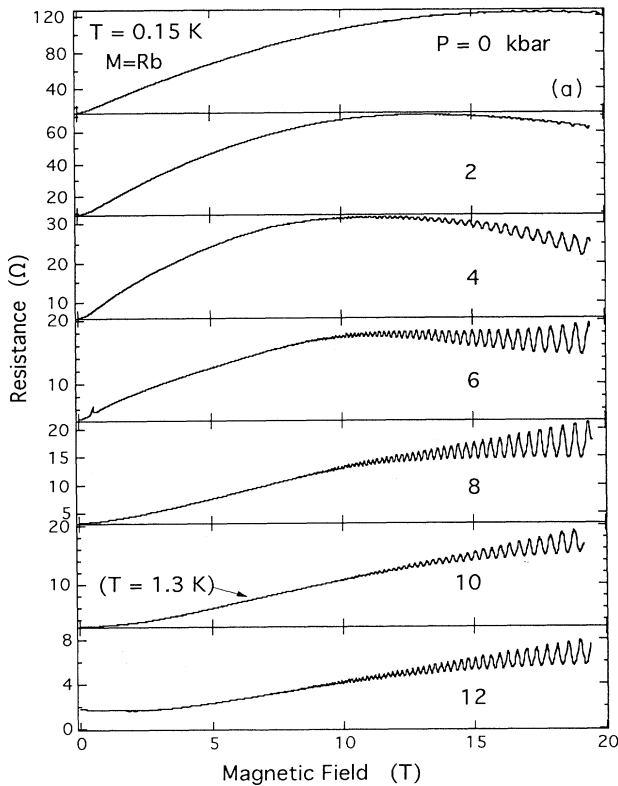


FIG. 8. (a) Pressure dependence of magnetoresistance and SdH oscillations in  $\alpha$ -(BEDT-TTF) $_2$ RbHg(SCN) $_{34}$  at 0.15 K (except as noted at 10 kbar). Note the resistance scales are different for different pressures. (See also Fig. 20 for detail of 6-kbar data.) (b) Details of the pressure-dependent SdH behavior at high fields. (Noise from the resistive magnet is present in some cases.) (c) Pressure-dependent FT spectrum of the SdH oscillations. (Splitting of the peaks is an artifact of the jitter in the magnetic field.)

is reduced to the field range of the measurements, as shown at 6 kbar [see also Fig. 20(a)]. Above 6 kbar magnetoresistance is always sublinear with field. Above 8 kbar, there is no evidence of the kink field, but the magnetoresistance at 12 kbar is even slightly negative below 5 T. The pressure dependence of the fundamental is  $dF_\alpha/dP = +11.74$  T/kbar, which corresponds to an increase in extremal orbit size of  $d \ln[S(P)]/P = 0.02/\text{kbar}$ . In Fig. 8(b) details of the pressure dependence of the SdH oscillation wave forms are shown, and the pressure-dependent FT spectra are given in Fig. 8(c). In the Fourier spectra there are distinguishable higher harmonic peaks, labeled here as  $2\alpha$  and  $3\alpha$ . Note that at 2 kbar, the  $2\alpha$  peak appears to be higher than  $\alpha$ . We have measured the MR and SdH oscillations between 0.15 and 3 K for each pressure to determine the effective mass  $m^*$  and Dingle temperature  $T_D$  for Rb. Within the experimental scatter neither has any systematic dependence on pressure:  $m^* = 1.5 \pm 0.2$  and  $T_D \approx 3.5$  K.

### B. Pressure studies of $\alpha$ -(BEDT-TTF)<sub>2</sub>KHg(SCN)<sub>4</sub>

The first member of the MHg family<sup>33</sup> studied in high magnetic fields was  $\alpha$ -(BEDT-TTF)<sub>2</sub>KHg(SCN)<sub>4</sub> (i.e.,  $M=K$ ). Typical ambient pressure behavior of the magnetoresistance and Shubnikov–de Haas effect is shown in Fig. 4. The FT gives details of the SdH oscillation frequencies, and harmonics of the fundamental up to sixth order and the magnetic breakdown orbit are observed. Here the frequency of the fundamental SdH oscillation frequency  $\alpha$  is 644 T. The ratio  $F_\alpha/F_\beta$  from Fig. 4(c)

yields an  $\alpha$  orbit that is 15% of the BZ. Other features mentioned in the Introduction are also evident, such as the appearance of the large second harmonic  $2\alpha$ , the very large MR with a maximum near 10 T, considerable hysteresis in the up and down field sweeps, and the signature of the “kink” transition. In Fig. 5 we show the pressure dependence of the MR and SdH data for K at 0.5 K for 1, 4, and 8 kbar. At 1 kbar, there is still a kink transition that occurs at the kink field  $H_{\text{kink}} \approx 22$  to 23 T and most features, including the strong second harmonic  $2\alpha$ , resemble those of the zero-pressure data. At 4 kbar the large MR starts to be suppressed, and its maximum appears at lower fields, as does the kink field. There is also considerable suppression of the second harmonic, and some indication of additional, low-frequency structure in the magnetoresistance. By 8 kbar, the MR maximum and kink field are completely suppressed, and there is a beating of the fundamental of frequency  $\sim 22$  T.

The pressure dependence of the fundamental frequency  $F_\alpha$ , shown in the inset of Fig. 5,  $d\alpha/dP = 12.1$  T/kbar, corresponding to a dependence of the Fermi surface area  $S(P)$  on pressure  $d \ln[S(P)]/dP = 0.019/\text{kbar}$ . The Dingle temperature ranges from 2 to 7 K (with no systematic pressure dependence), corresponding to a level broadening of  $\approx 4$  meV. The effective mass related to the SdH oscillations is found to be pressure independent within the experimental scatter:  $m^* = (1.4 \pm 0.4)m_0$ .

### C. Pressure studies of $\alpha$ -(BEDT-TTF)<sub>2</sub>TlHg(SCN)<sub>4</sub>

We now turn to the final nonsuperconducting member of the family we have investigated,  $\alpha$ -(BEDT-

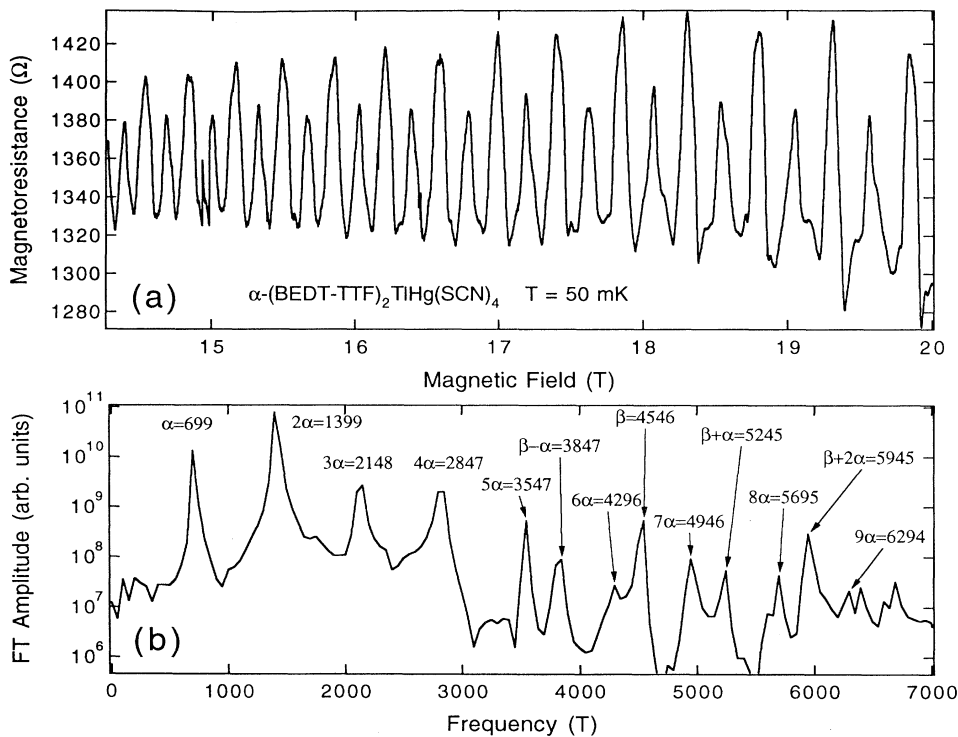


FIG. 9. Ambient pressure SdH behavior in  $\alpha$ -(BEDT-TTF)<sub>2</sub>TlHg(SCN)<sub>4</sub> at 0.05 K. (a) Oscillatory magnetoresistance (background MR subtracted) between 14 and 20 T in a superconducting magnet. Here, in addition to the oscillations associated with the  $\alpha$  and  $2\alpha$  orbits, the breakdown orbit  $\beta$  is clearly visible even in a conventional non-field-modulation transport measurement. (b) FT of SdH oscillations over a wide range of frequency showing harmonic, combination, and breakdown orbits.

$(\text{TTF})_2\text{TIHg}(\text{SCN})_4$  (i.e.,  $M=\text{TI}$ ). Recent pulsed field work and hybrid magnet work<sup>55</sup> show the kink field for  $M=\text{TI}$  at ambient pressure to be above 23 T. Our work has focused on measurements below 20 T. We observed, at ambient pressure, magnetic breakdown (MB) in this material in a 20-T superconducting magnet by the SdH effect using standard magnetic-field sweeps, as shown in Figs. 9(a) and 9(b). As first observed by Uji *et al.* for  $M=\text{K}$ ,<sup>37</sup> this frequency (which represents the area of the first BZ) is clearly observable. [See also Fig. 4(c) for

$M=\text{K}$ .] The ability to measure the breakdown orbit made the prospects of studying such effects under pressure very promising. In addition to the pressure dependence of the closed orbit  $\alpha$  and its harmonics, the  $\beta$  frequency and amplitude could also be determined. Hence information of the pressure dependence of the BZ size, and on the proximity of the hole band to the electron band, could be measured.

Our pressure-dependent study for  $M=\text{TI}$  is in two parts. The first is in a Bitter magnetic to 20 T, where the

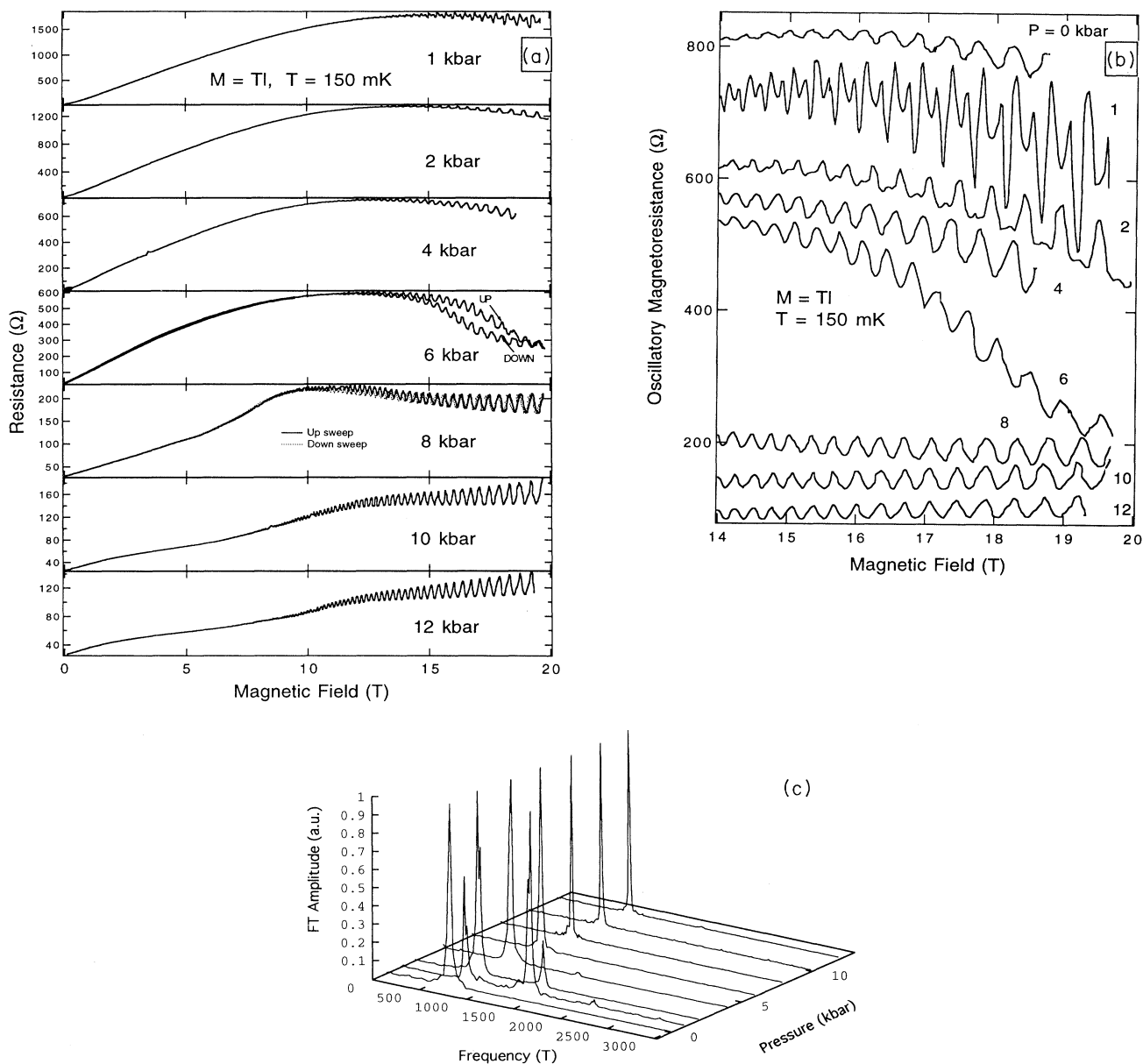


FIG. 10. (a) Pressure dependence study of the magnetoresistance and SdH oscillations in  $\alpha$ -(BEDT-TTF) $_2$ TIHg(SCN) $_4$  in a Bitter resistive magnet at 0.15 K. At low pressures, the kink field is not observed due to the 20-T limit of the magnet. (See Fig. 20 for details of the hysteresis at 8 kbar.) (b) Details of the pressure-dependent SdH oscillation wave forms at high fields. (Jitter in some of the sweeps came from fluctuations in the magnet sweep output.) (c) Pressure dependence of the FT spectrum of the SdH oscillations. (Splitting of the peaks is an artifact of the jitter in the magnetic field.)

field noise was not low enough to observe magnetic breakdown. The second was in a superconducting 20-T magnet. A different sample was used in each study. In Fig. 10(a) we present a systematic study for Tl from 0 to 12 kbar in the Bitter magnet system for a sample of 6-k $\Omega$  resistance along the  $b$  axis at room temperature, and with a resistivity ratio  $R(300\text{ K})/R(1\text{ K})=160$ . The features are very similar to those of both the K and Rb salts. The kink field behavior is clearly visible, including the hysteretic behavior at 6 kbar, where the kink field is within range of the accessible fields. Other aspects like the MR curvature, the SdH oscillations, harmonic behavior, and their variation with pressure are further brought out in Figs. 10(b) and 10(c). We see that  $H_{\max}$  decreases with pressure, and that there is an onset of new features in the low-field magnetoresistance above 6 kbar. These new features, especially by 12 kbar, appear to be a very low-frequency SdH oscillation. In Fig. 10(c) the second harmonic is largest at nonzero pressure. In a manner similar to the  $M=\text{Rb}$  data, we believe this is due to a more ideal stabilization of the hydrostatic nature of the pressure at pressures slightly greater than those near ambient conditions. The increase of the fundamental SdH oscillation

frequency  $\alpha$  with pressure is  $dF_{\alpha}/dP=9.2\text{ T/kbar}$ , which corresponds to the increase in the Fermi surface area of  $d\ln[S(P)]/dP=0.014/\text{kbar}$ . With increasing pressure, the second harmonic is reduced significantly. The effective mass and Dingle temperature were not systematically studied for Tl, but there was no evidence for a strong pressure dependence of either parameter in this case. The MR behavior of the Tl salt is similar to that of the Rb and K salts. The MR at 0 kbar rises from 37  $\Omega$  at zero field to a maximum of 1600  $\Omega$  at 15.4 T. The ratio  $\Delta R/R(0)$  is nearly 40. As the pressure is increased, the giant MR decreases, and the field position and magnitude of  $\Delta R$  shifts to lower values.

The second set of measurements were carried out in a 20-T superconducting magnet, where sufficient resolution was available to study the magnetic breakdown effects. At ambient pressure, in the first sample measured we observed [see Fig. 9(b)] a remarkable number of harmonics of the fundamental frequency  $\alpha$ , the magnetic breakdown orbit  $\beta$ , and the combinations  $\beta-\alpha$ ,  $\beta+\alpha$ , and  $2\beta+\alpha$ . The ratio  $F_{\alpha}/F_{\beta}$  from Fig. 9(b) yields an  $\alpha$  orbit that is 15% of the BZ. In the second sample measured the pressure was increased incrementally from 0 to 8 kbar, and

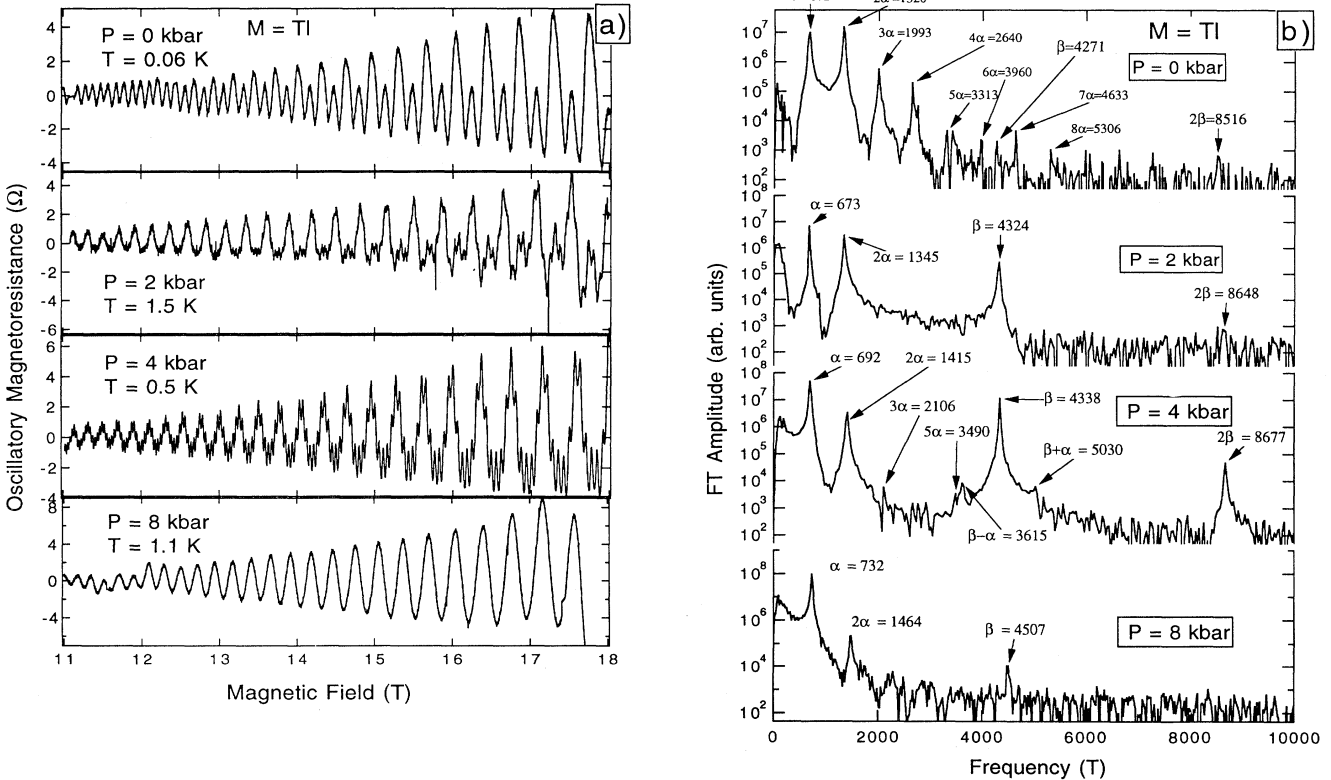


FIG. 11. (a) Pressure-dependent study of the SdH behavior of  $\alpha\text{-(BEDT-TTF)}_2\text{TIHg(SCN)}_4$  in a 20-T superconducting magnet. Here the amplitude of the breakdown orbit  $\beta$  becomes unusually large at 4 kbar. (b) FT spectra of pressure-dependent SdH oscillations. The amplitude of the  $2\alpha$  harmonic decreases monotonically with pressure, whereas the amplitude of the magnetic breakdown orbit  $\beta$  is observed to first increase, then decrease with pressure. Note that since the temperatures were not the same [see (a)] for each pressure, comparisons of the FT amplitudes of the different orbits must be made relative to each other for a particular FT spectrum.

the results are shown in Fig. 11(a). (Technical difficulties made dilution refrigerator temperatures inaccessible in some cases.) Apparent in Fig. 11(b) is that the second harmonic decreases monotonically with increasing pressure. The amplitude of the magnetic breakdown signal, however, increases dramatically up to 4 kbar, and then decreases again as 10 kbar is reached. (The frequency of  $\beta$  increases monotonically.) To see if the  $\beta$  orbit would again appear at higher pressures, we increased the pressure to 12 kbar (14 kbar at room temperature), the limit of the pressure clamp range. The magnetoresistance data are shown in Fig. 12. At 12 kbar  $\beta$  was not at all evident, and our results therefore at present all point to a decrease of the magnetic breakdown probability between the closed- and open-orbit bands at high pressure.

Referring again to Fig. 12, two results emerged. The first is that the fundamental  $F_\alpha$  frequency can be observed down to a field of less than 2.6 T. Based on the observations of Uji *et al.*,<sup>38</sup> in the LTS where the Fermi surface is reconstructed, the overlapping hole orbits

create a magnetic breakdown network of many smaller orbits, and the original  $\alpha$  orbit itself becomes a magnetic breakdown orbit due to its many intersections with other  $\alpha$  orbits [see Fig. 3(a)]. At ambient pressure, in the LTS, the  $\alpha$  orbit is not observable below about 4 T, even with the field modulation method, due to the low magnetic breakdown probability at that field. Only the much smaller orbits associated with the reconstructed Fermi surface are visible in this limit. Hence Fig. 12 implies that pressure has removed all vestiges of the LTS reconstructed state, and the  $\alpha$  orbit is again a closed orbit without intersections with other orbits. The second observation is the very pronounced slow oscillation. This we believe is another example of pressure-induced imperfect nesting of the open-orbit sheets. Field modulation and angular-dependent magnetoresistance studies are needed to fully understand the effects that such high pressures have on the Fermi-surface topology.

#### D. Pressure studies of $\alpha$ -(BEDT-TTF)<sub>2</sub>NH<sub>4</sub>Hg(SCN)<sub>4</sub>

Our investigation of the MR and SdH oscillations  $\alpha$ -(BEDT-TTF)<sub>2</sub>NH<sub>4</sub>Hg(SCN)<sub>4</sub> (i.e.,  $M$ =NH<sub>4</sub>) under pressure are extensive, and some results have been previously reported.<sup>56</sup> There are some anticipation, based on the larger unit cell, that pressure would destroy the superconducting state and stabilizes the LTS state seen for  $M$ =Rb, K, or Tl. Superconductivity was suppressed, as shown in Fig. 13, but the new normal state has a form different from the LTS. We divide this section into four subsections dealing with the fundamental SdH oscillation, the slow SdH oscillation, the background MR, and the superconductivity.

The most important data, the MR and SdH oscillations for different pressures at 150 mK are presented in Fig. 14, where the  $\alpha$  SdH oscillations, anomalous slow SdH oscillations, superconductivity, and the sublinear background MR behavior are present. The “0” pressure data represent the sample in the pressure clamp+fluid with finger-tight pressure at room temperature. Here the SdH oscillations are of frequency 579 T, compared to 568 T previously measured in ambient pressure. The ratio  $F_\alpha/F_\beta=557\text{ T}/4212\text{ T}$  from pulsed field data to 51 T (where the  $\beta$  orbit was observed for the first time in the NH<sub>4</sub> material<sup>57</sup>) yields an  $\alpha$  orbit that is 13.2% of the BZ, which is significantly less than the average of 15% for the DW salts. This is consistent with the notion that very high magnetic fields are needed to observe the  $\beta$  orbit for NH<sub>4</sub> since the smaller closed orbit places the open- and closed-orbit bands further away from each other in  $k$  space (see Sec. VIB below). No anomalous high second harmonic amplitude like that in the K, Rb, and Tl salts has been found in this NH<sub>4</sub> salt at any pressure studied. The  $\alpha$  orbit area expands with increasing pressure as  $d \ln S(P)/dP=0.03/\text{kbar}$ . The pressure dependence of the effective mass is  $m^*=2.1m_0$  at 0 kbar (see note in Ref. 56),  $1.7m_0$  at 2 kbar; and for pressures greater than 4 kbar, the effective mass values (within the experimental scatter) are essentially pressure independent, namely,  $m^*=(1.5\pm 0.1)m_0$ . Hence at high pressures above 4 kbar  $m^*$  for  $M$ =NH<sub>4</sub> is a similar to that obtained for the

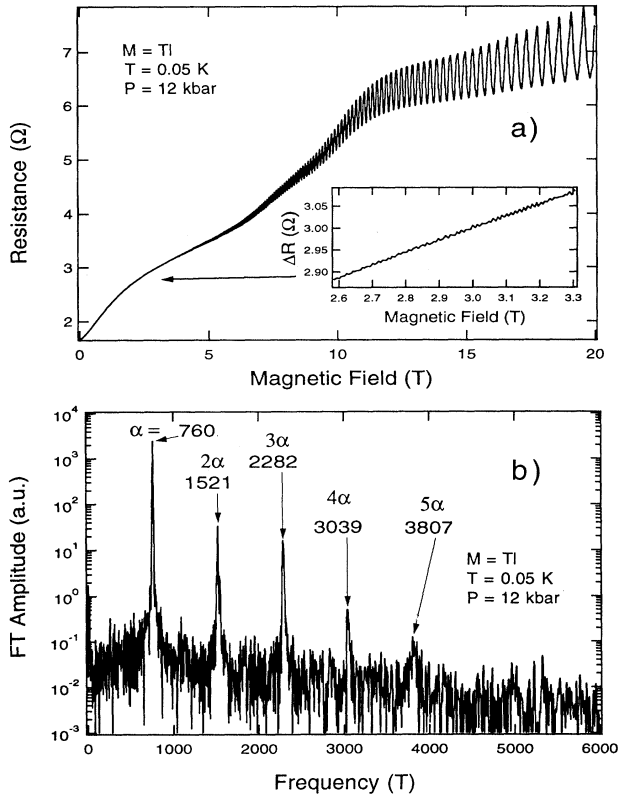


FIG. 12. Study of  $\alpha$ -(BEDT-TTF)<sub>2</sub>TiHg(SCN)<sub>4</sub> at 12 kbar in a 20-T superconducting magnet. (a) Magnetoresistance and SdH oscillations at 0.05 K. The fundamental frequency  $F_\alpha$  dominates the behavior, and the inset shows the lowest onset field ( $\approx 2.4$  T) of SdH oscillations ever observed in  $\alpha$ -(BEDT-TTF)<sub>2</sub>MHg(SCN)<sub>4</sub> materials. A slow oscillation of frequency 20 T is also clearly visible on the background magnetoresistance. (b) The FT spectrum of the SdH oscillations shows only the peaks for the regular fundamental harmonic and its multiples. No magnetic breakdown peak  $\beta$  is found at this pressure.

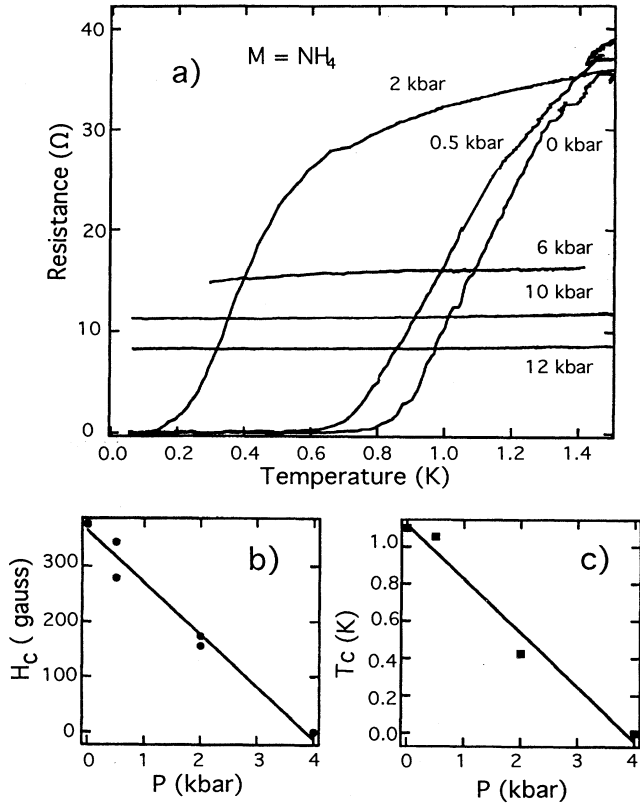


FIG. 13. Superconductivity in  $\alpha$ -(BEDT-TTF) $_2$ NH $_4$ Hg(SCN) $_4$ . (a) Pressure dependence of resistance near the superconducting transition in  $\alpha$ -(BEDT-TTF) $_2$ NH $_4$ Hg(SCN) $_4$ . (b) Pressure dependence of the upper critical field. (c) Pressure dependence of  $T_c$ .

DW salts. The Dingle temperature averaged over all pressures is  $T_D = 1.7$  K. The only complex behavior of the  $\alpha$  orbit in the NH $_4$  salt is a beatlike behavior at 2 and 4 kbar as shown Fig. 15 (also shown at 4 kbar for another sample). We found the difference between the two oscillation frequencies to be 79.2 T at 2 kbar and 43.4 T at 4 kbar (52.0 T in the second sample). If we ascribed the beating to the warping of the cylindrical FS along the  $b$  axis, this corresponds to a transfer energy of  $t_b \approx 0.06t_{a-c}$  and  $t_b \approx 0.03t_{a-c}$  for the 2- and 4-kbar cases, respectively.

The anomalous slow SdH oscillation behavior in the NH $_4$  salt under pressure that we observed was the first clear indication that significant alteration of the electron structure beyond the simple expansion of the closed-orbit areas was possible. In Fig. 14, one can see in the intermediate pressure range, as the arrows indicate, that there exists a new series of oscillations superimposed onto the monotonically arising MR background and the fast SdH oscillations. In Fig. 16(a), the Landau indices for the anomalous slow oscillations versus inverse field are shown for different pressures. The integer indices are assigned to the resistance maxima while the half integers

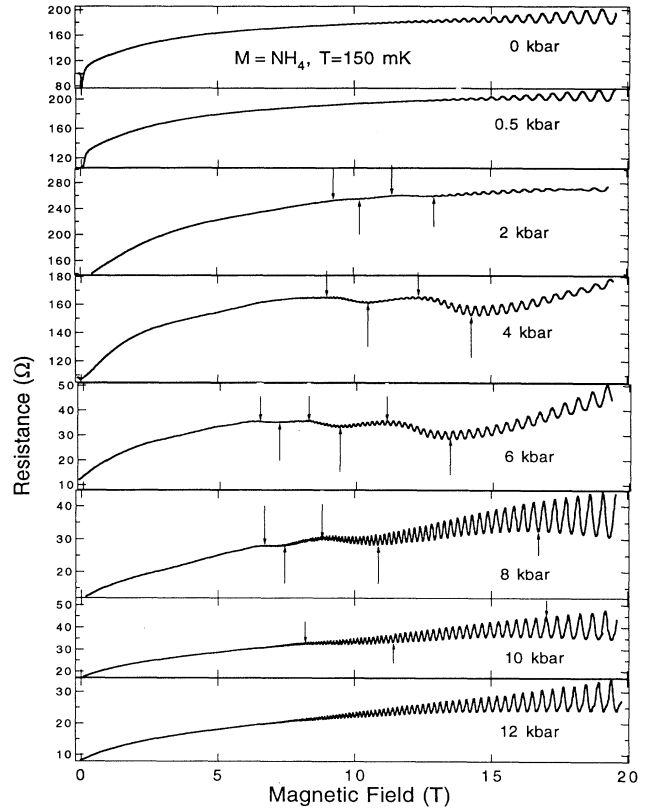


FIG. 14. Pressure dependence of magnetoresistance and SdH oscillations of  $\alpha$ -(BEDT-TTF) $_2$ NH $_4$ Hg(SCN) $_4$  at 150 mK. The superconducting transition is indicated at low pressures, and the arrows refer to the half cycles of the slow oscillations.

are assigned to minima. The linear fits in Fig. 16(a) demonstrate the periodicity in  $1/H$ , and yield the SdH oscillation frequency of the slow oscillations. The pressure dependencies of  $F_\alpha$  and the slow oscillation frequency  $F_{\text{slow}}$  are shown in Fig. 16(b). The opposite pressure dependencies for the slow and fast oscillations are  $dF_{\text{slow}}/dP = -3.6$  T/kbar and  $dF_\alpha/dP = 16.7$  T/kbar, respectively. Although the magnitudes of these two pressure dependencies are comparable, there is no simple explanation one can envision from the band-structure picture of Mori *et al.*,<sup>1</sup> hence, a new type of small closed orbits must have arisen from the Fermi-surface topology change under pressures. Our best estimate from the limited range of data available for the slow oscillations is that the effective mass  $m_{\text{slow}}^* \approx 1.9m_0$ . The Dingle temperature  $T_D \approx 1.4$  K is low, allowing the slow oscillation to exist at temperatures up to 2 K. We observed that the slow oscillation Landau level position is sensitive to temperature as shown in Fig. 17 compared with the  $\alpha$  oscillations, which do not shift in field position with temperature.

The background MR structure in the NH $_4$  salt displays a different character than that in the K, Rb, and Tl salts. There is no giant MR. The background MR monotonically

cally increases for all pressures investigated with a sub-linear dependence on magnetic field. The largest MR increase at 0, 0.5, and 2 kbar is only about 10% of the room-temperature resistance.

The pressure effect on superconductivity in  $\text{NH}_4$  is to reduce  $T_c$  to zero by 4 kbar, as shown in Fig. 13 (see also Fig. 23). We observe that  $dT_c/dP \approx -0.25$  K/kbar and  $dH_{c2}/dP \approx -100$  G/kbar.  $dT_c/dP$  is an order of magnitude larger than the pressure dependence of  $T_c$  in simple metals.

## VI. DISCUSSION

### A. Pressure effects on the Q2D band and the first Brillouin zone

A summary of the pressure dependence of the oscillation frequencies is shown in Fig. 18. The pressure dependence of the fundamental hole orbit frequency  $F_\alpha$  is the

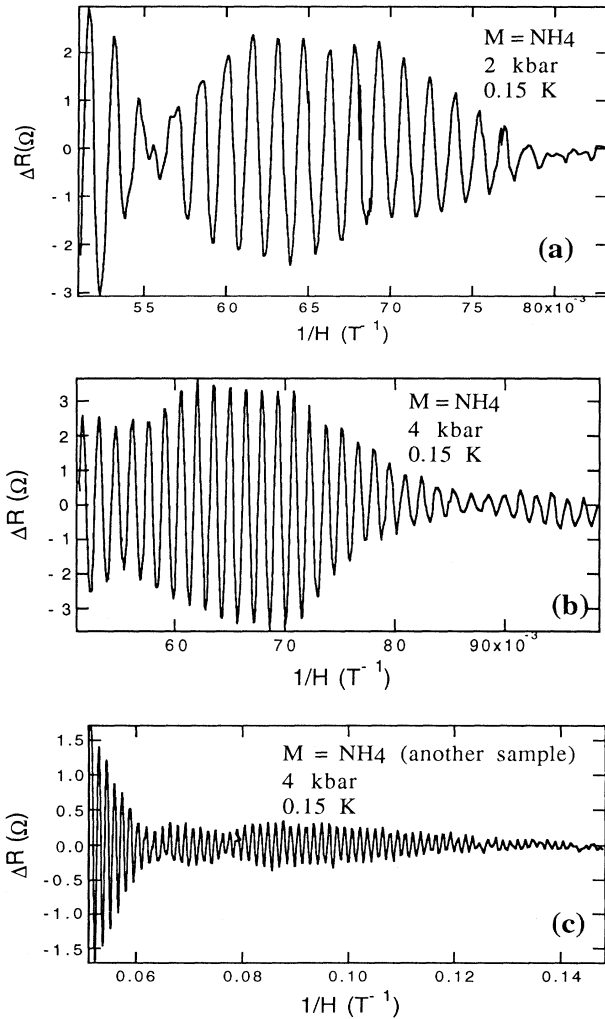


FIG. 15. Elucidation of the beat structure in the oscillatory magnetoresistance  $\Delta R$  of  $\alpha\text{-(BEDT-TTF)}_2\text{NH}_4\text{Hg(SCN)}_4$  under pressure. (a) 2 kbar, (b) 4 kbar, and (c) 4 kbar (a second sample).

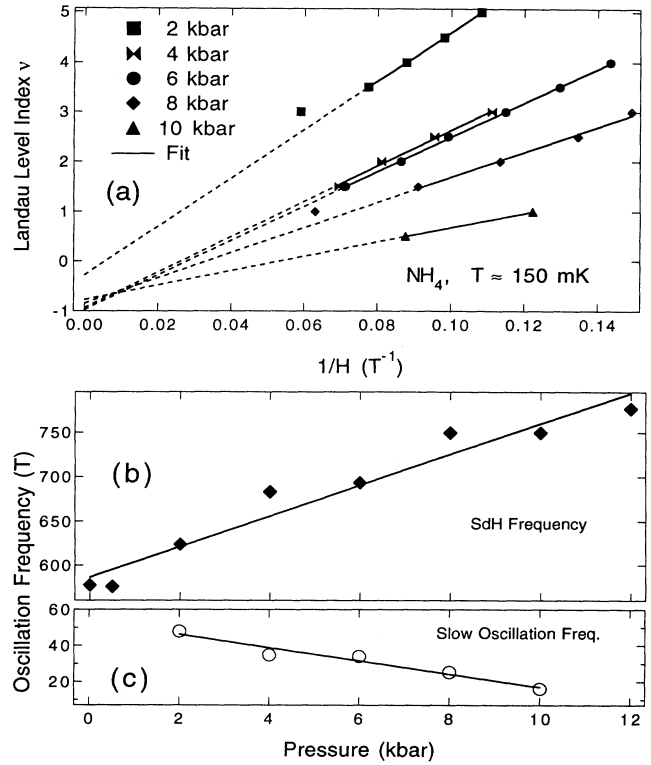


FIG. 16. (a) Landau index of slow oscillations in  $\alpha\text{-(BEDT-TTF)}_2\text{NH}_4\text{Hg(SCN)}_4$  for different pressures at 150 mK. (b) Pressure dependence of the fundamental and slow oscillation frequency.

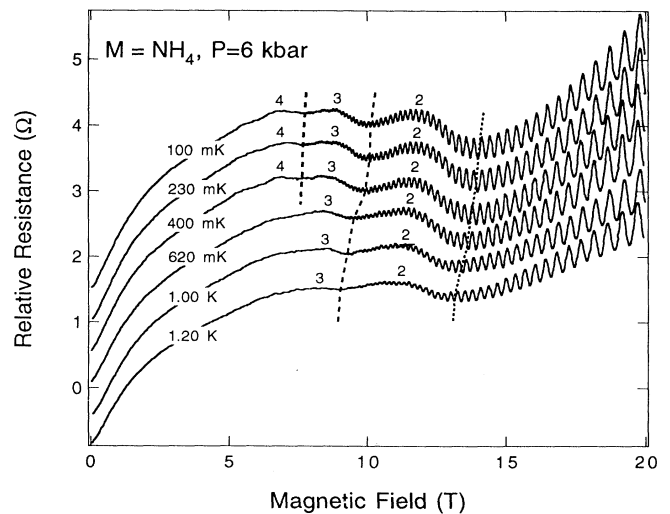


FIG. 17. Temperature variation for the slow oscillation positions in  $\alpha\text{-(BEDT-TTF)}_2\text{NH}_4\text{Hg(SCN)}_4$  with temperature. Indices refer to the corresponding Landau level maxima, and dashed lines follow the temperature dependence of the Landau level minima.

most accessible gauge of how pressure affects the band structure. We find that hydrostatic pressure increases  $F_\alpha$  in all cases studied as expected from the tight-binding model with two equally filled bands. In the case of the DW salts, the extremal area of the  $\alpha$  orbit increases with pressure in the range 1.5%–2.0%/kbar, and we find no measurable pressure dependence of the effective mass  $m^*$ . This is essentially a result of the insensitivity of the product of the bandwidth and lattice constant  $t_a a^2$  in the TBM to pressure. In the case where the magnetic breakdown orbit  $\beta$  (which involves the entire BZ) was studied for  $M=\text{TI}$ , the expansion of the BZ area with pressure was 0.5%/kbar. For  $\text{NH}_4$ , the increase in  $F_\alpha$  is more substantial (3.5%/kbar) here the ambient pressure frequency is the lowest, but the frequency approaches that of the DW salts at high pressure. Here we observed a measurable change in effective mass from  $2.1m_0$  at ambient pressure to  $1.5m_0$  at 4 kbar. Above 4 kbar the

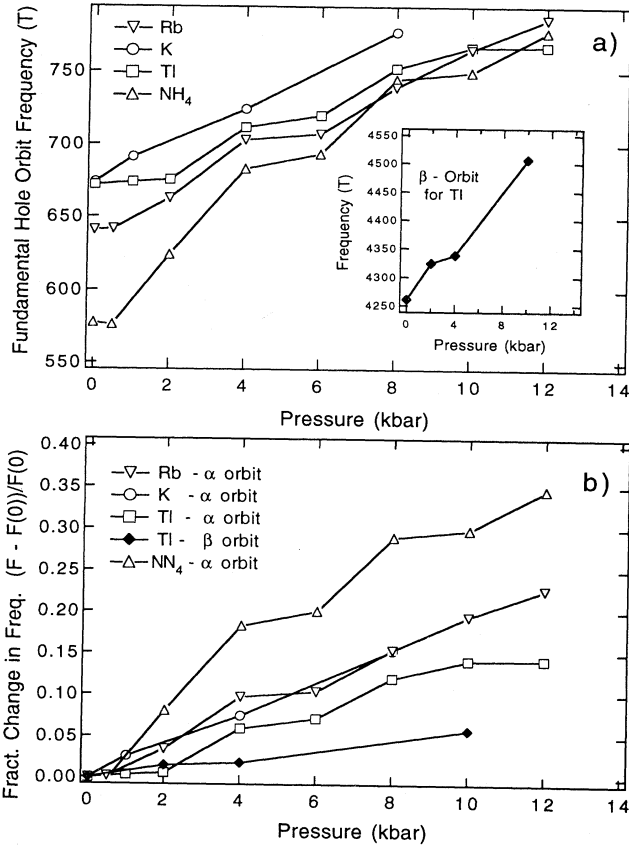


FIG. 18. Pressure dependence of extremal orbits in  $\alpha$ -(BEDT-TTF) $_2$ MHg(SCN) $_4$ . (a) Pressure dependence of  $\alpha$  orbit frequencies. Inset:  $\beta$  orbit, which is proportional to first BZ area. (b) Fractional change in  $\alpha$  and  $\beta$  orbits with pressure. Deviations from smooth monotonic behavior most likely arise from uncertainties in the values of pressure at low temperature, the absolute orientation of the  $b$ -axis of the sample within the pressure cell with respect to magnetic-field direction, and the necessity to thermally cycle the sample to room temperature to increase the pressure.

effective mass for  $M=\text{NH}_4$  did not change significantly from  $1.5m_0$ . We interpret the pressure dependence of the effective mass for  $M=\text{NH}_4$  as follows:  $m^*$  is enhanced when superconductivity is present, but when pressure removes the superconducting state, the mass returns to the “normal” effective mass seen in the nonsuperconducting DW materials, which is in the range  $1.4m_0$ – $1.8m_0$ .

We may use the pressure dependence of the  $\alpha$  and  $\beta$  orbit areas to gain insight into the actual changes in the Fermi surface with pressure. In Fig. 19(a) a comparison of the BZ at 0 and 10 kbar, based on our results, is drawn to scale. To simplify the FS topology we have assumed the  $a$  and  $c$  axes to be equal, and the hole and electron Fermi surfaces to be dispersionless circular cylinders and parallel sheets, respectively. Since only the hole and BZ area can be determined from our data, we have used the charge-transfer criterion to set the pressure-dependent area of the electron FS equal to that of the pressure-dependent hole FS. Precise determinations<sup>37</sup> of  $\alpha$  and  $\beta$  at zero pressure indicate this equality. Here we have assumed that the effective mass is pressure independent, based on the tight-binding and experimental results.

In Fig. 19(b) we show the pressure-dependent form of the simplified tight-binding band structure near the Fermi level again drawn to scale, based on our results. We have estimated  $E_F$  from the  $F_\alpha$  frequency. Note that although the Fermi level rises, the hole band also expands

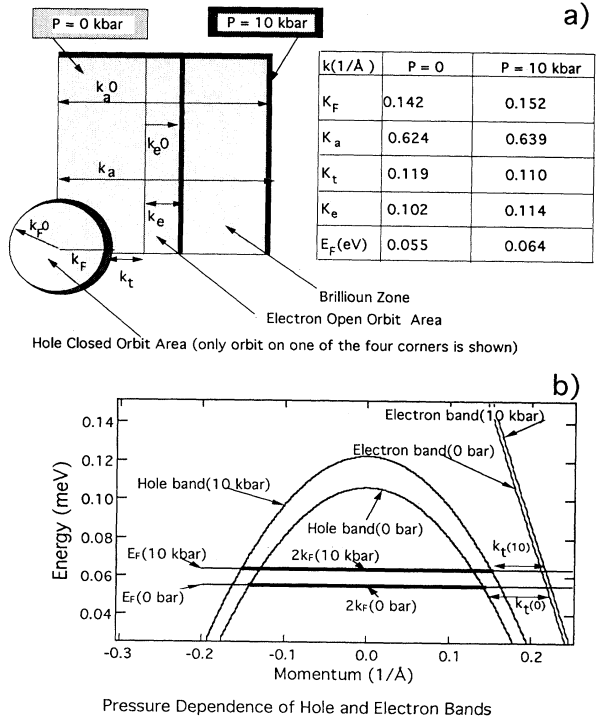


FIG. 19. Pressure dependence of Fermi surface and band structure in  $\alpha$ -(BEDT-TTF) $_2$ MHg(SCN) $_4$ . (a) Description of the main Fermi surface features at 0 and 10 kbar. (b) Behavior of hole and electron bands near the Fermi level.

in such a way as to give the observed increase in the closed-orbit area. A similar case must hold for the electron band. If we still maintain the assumption of a pressure-independent effective mass, then there are three parameters that determine the behavior in Fig. 19(b): the Fermi level  $E_F$ , the Brillouin zone size  $k_{\text{BZ}}$ , and the tight-binding bandwidths  $t$ . In the approximation of parabolic hole and electron bands, we estimate the pressure dependence of the hole and electron bandwidths to be  $dt_h/dP \approx 1.6$  meV/kbar and  $dt_e/dP \approx 0.06$  meV/kbar.

Pressure-induced beating effects of the fundamental frequency have been observed, particularly in the case for  $M=\text{NH}_4$ . This effect can occur when there are two slightly different extremal orbits present due to a warping of the closed-orbit cylindrical Fermi surface along the least conducting direction due to a small, but finite transfer energy  $t_b$ . Hence a simple explanation for pressure-induced beating effects is that application of pressure drives the system towards a more 3D character, i.e., a larger  $t_b$ . We can estimate the increase in warping ( $\Delta t_b$ ) of the cylinders associated with the fundamental orbit. On average, for  $\text{NH}_4$  the beat frequency increased by 20 T/kbar. From the relation  $\Delta(t_b/t_{a-c}) = \Delta F/2F$ , where  $t_{a-c}$  is the transfer energy in the  $a$ - $c$  plane, the pressure dependence of the warping of  $t_b$  is of order  $\sim 2\%$  per kbar of the in-plane transfer energies.

### B. Relative pressure dependence of Q1D and Q2D bands

In the simple picture, pressure expands the BZ and its topology uniformly since  $k$  space increases for decreasing real-space dimensions. Hence the tunneling probability (Blount model<sup>8</sup>)  $P_t \approx \exp(-H_0/H)$  of carriers between the closed and open orbits (magnetic breakdown) should decrease with pressure, since the momentum gap  $k_t$  between the bands should increase. Here  $H_0 = mE_g^2/e\hbar E_F$ , where  $E_g$  is the effective tunneling gap energy determined by the momentum gap  $(\hbar k_t)^2/2m$ . However, we know from the present work that the extremal area of the  $\alpha$  orbit increases with pressure (and so must the enclosed area associated with the open-orbit sheets due to charge transfer) at a rate greater than the BZ area ( $\beta$  orbit). Hence the pressure dependence of  $k_t$  may actually decrease as the results of Fig. 19(a) suggests for the pressure range 0–10 kbar. For example, by using the above relations and the values in Fig. 19(a), the breakdown probability increases by a factor of 5000 between 0 and 10 kbar at a field of 20 T. We recall from Figs. 11 and 12 that the pressure dependence of the amplitude of the  $\beta$  orbit shows a maximum around 4 kbar. In this pressure range  $k_t$  may decrease due to anisotropy in the pressure dependence of the transfer energies,<sup>50</sup> thereby increasing the breakdown probability. At high pressures, however, the amplitude of the  $\beta$  orbit diminishes, and is essentially absent by 12 kbar. Hence the highest pressure data are consistent with the simple expanding BZ picture. Without an independent, direct measurement of the changes in the open orbit topology, it is difficult to pin down the exact pressure dependence of  $k_t$ . There is an alternative explanation for the nonmonotonic pressure dependence of

the  $\beta$  orbit amplitude. Since the  $\beta$  orbit is characteristic of the metallic, and not the DW Fermi surface, as pressure destroys the DW, the contribution of the metallic phase (and therefore the  $\beta$  orbit contribution) increases. Ultimately the decrease in the  $\beta$  amplitude at the highest pressure may result from the increase in  $k_t$  due to the expanding BZ. Independent measurements<sup>58</sup> between 9 and 50 kbar by the diamond anvil technique do not show evidence for the  $\beta$  orbit. This is an indication that  $k_t$  is larger than the ambient pressure value in this pressure range. More work at higher pressures will be needed to sort out these possibilities.

A quantitative estimate of the tunneling probability  $P_t$  based on  $k_t$  derived from the band calculation indicates that the field  $H_0$  is of order 500 T at ambient pressure. For  $H=H_0$  the tunneling probability is 37%, far in excess of what is actually needed to observe an orbital frequency in a FT spectrum. Oscillations can be seen at significantly lower fields than  $H_0$ . For example, in Fig. 4(c) we see that the amplitude of  $\beta$  is down by 4 orders of magnitude from the  $\alpha$  orbit; i.e.,  $P_t \approx 0.01\%$ . Even though breakdown oscillations with very small probabilities can be seen experimentally, the observed breakdown field of  $\approx 6$  T for  $\beta$  seems anomalously low when compared with  $H_0=500$  T. Recent AMRO studies in the metallic phases of these materials<sup>9,59,34</sup> indicate an elliptical shape for the closed orbit. The eccentricity is in the range 1.5–2, and if this eccentricity is in the direction of the open-orbit sheets, the tunneling probability is substantially increased. An eccentricity of, say, 1.75 gives a  $k_t$  of  $0.075/\text{\AA}$  with a  $H_0=75$  T. This would put the probability within the range of observation. Hence consideration of the elliptical nature of the closed orbits can help resolve the large difference between the observed and predicted breakdown fields.

It is tempting to consider that the  $\beta$  orbit arises from some aspect of the reconstructed Fermi surface. We do not think that this is possible for several experimental reasons. First, the rate of increase in the  $\alpha$  orbit area is three times that of the  $\beta$  orbit. This implies that the  $\beta$  orbit is not a combination of  $\alpha$  orbits in the reconstructed scheme shown in Fig. 1. It is a property of the metallic, unreconstructed FS. Indeed, the linear compressibility deduced from the  $\beta$  orbit pressure dependence is  $\kappa_a = -0.0024/\text{kbar}$ , which is in good agreement with other reports of  $\kappa_a$  for the BEDT-TTF materials.<sup>48</sup> Second, a detailed experimental investigation<sup>38</sup> of the frequencies that arise from the reconstructed Fermi surface is inconsistent with the notion that the  $\beta$  orbit arises from the reconstruction. Third, the  $\beta$  orbit is observed for  $M=\text{NH}_4$  (where no reconstruction occurs) in pulsed magnetic fields.<sup>57</sup> The experimental magnetic breakdown threshold for  $\text{NH}_4$  is of order 30 T, a result consistent with the greater separation of the hole and electron bands in this material.

Based on the discussion above, the computed tunneling probability [based on the Fermi-surface topology in Fig. 2(d)] for magnetic breakdown between open and closed orbits seems anomalously low when compared to the significant amplitude of the  $\beta$  orbit observed in these ma-

terials. However, present band calculations might not reflect accurately enough the momentum gap between the bands. Indeed different treatments of the band structure in the  $\alpha$ -(BEDT-TTF)<sub>2</sub>MHg(SCN)<sub>4</sub> series give a number of different topologies. In the extended Hückel method the molecular orbitals are approximations, and it is possible that important details have either been approximated or omitted in the band calculations. It is also possible that the tunneling mechanism is more complicated than the Blount model and other channels exist that raise the probability. Finally, the composition of the molecular orbitals (which are constructed from the atomic orbitals) may change with increasing field, and new tunneling channels may open. Clearly this is an exciting area and further attention is warranted.

### C. Pressure effects on the Q1D band

The Q1D band area must expand with pressure as the Q2D band area does if indeed the charge transfer locks the Q2D and the Q1D bands at equal filling. Although the open orbit cannot be probed directly via the SdH effect, the pressure dependence of the  $\beta$  orbit, which involves the open-orbit sheets, is consistent with this expectation.

More interesting is the phenomenon of pressure-induced “slow oscillation” behavior in all materials studied. In the case  $M$ =Tl (Fig. 10 and 12) and  $M$ =NH<sub>4</sub> (Figs. 14 and 17), they were quite pronounced. For  $M$ =K (Fig. 5) and  $M$ =Rb (Fig. 8) they were less pronounced but could still be seen as changes of slope in an otherwise smoothly varying background resistance. Similar behavior at ambient pressure has been reported<sup>60</sup> in  $\alpha$ -(BEDT-TTF)<sub>2</sub>TlHg(SeCN)<sub>4</sub> at ambient pressure, and for  $\alpha$ -(BEDT-TTF)<sub>2</sub>KHg(SCN)<sub>4</sub> under uniaxial stress.<sup>61</sup> The slow oscillations may arise from imperfect nesting of the open orbits, which results in small closed pockets on the Fermi surface. Due to anisotropy in these materials, pressure may produce a small difference in the FS topology of the open-orbit sheets, which in turn modifies the nesting condition. It is difficult to identify other mechanisms to explain this effect, at least based on the calculated band structure of Fig. 2. Since we estimate that it would take 100 kbar or more to lift, say, the bottom of the electron band up to the Fermi level, this kind of effect is unlikely to yield the small pockets observed. Similarly, there are no other bands near the Fermi level, which could cross in the range of pressures we have studied. The slow oscillation behavior persists at pressures above  $P_c$ , and is therefore not related to the LTS. This leaves imperfect nesting of the open sheets the most plausible cause. An exciting possibility exists here. The slow oscillations are in the second Landau level at high fields, very near the quantum limit, and in some cases, it is clear that the background magnetoresistance is strongly influenced by this effect. With the appropriate choice of pressure and high magnetic field, it should be possible to explore the quantum limit (i.e., quantum Hall effect) in these small pockets.

### D. Pressure effects on the low-temperature state

The phase boundary between the metallic and density-wave states is generally thought to be the pressure-dependent resistivity anomaly at  $T_{DW}(P_c)$  for zero magnetic field, and the pressure-dependent kink field  $H_{kink}(P_c)$  anomaly at finite fields. This definition leads to the phase diagram shown in Fig. 1(a), which is based on work reported here as well as that of other workers. There are several caveats in defining the phase diagram. First, there is some evidence that below about 1 K, above  $H_{kink}(P_c=0)$ , there may be another phase that is not a simple metallic phase,<sup>15</sup> but further high-field work is needed to clarify the question. Second, the reported  $T_{DW}(P_c)$  for Tl (Ref. 17) suggests a lower  $P_c$  (about 3 kbar) than our  $H_{kink}(P_c)$  results suggest. Here  $P_c$  is the critical pressure at the boundary. Hence although it seems evident that  $T_{DW}(P_c)$  and  $H_{kink}(P_c)$  are the same boundary, the connection is not unambiguous. Regarding  $H_{kink}(P_c)$ , we make note of the hysteretic behavior in Fig. 20. Here the last vestiges of the hysteresis associated with the kink field behavior are shown for  $M$ =Rb (6 kbar) and  $M$ =Tl (8 kbar). It is noteworthy that the pressures quoted are the room-temperature values *less* the 2-kbar (rule of thumb) correction for low-temperature adjustment. Therefore there is little doubt that the density-wave state is still evidence up to these pressures, well above 3 kbar, at least at low temperatures where the measurements were made. At slightly higher pressures, the kink field behavior (hysteresis and drop in magnetoresistance) and the magnetoresistance maximum “fade out.”

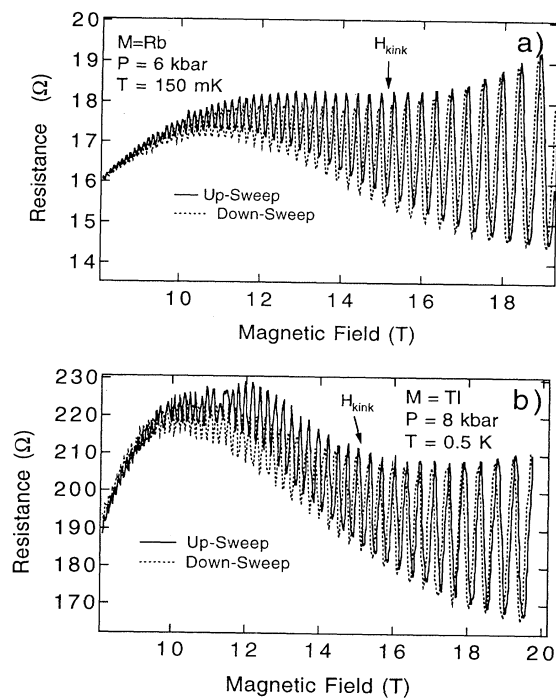


FIG. 20. Hysteretic behavior in magnetoresistance and kink field at high pressures for  $M$ =Rb and  $M$ =Tl near  $P_c$ .

$H_{\text{kink}}(P)$  and  $H_{\text{max}}(P)$  cannot be followed to zero field at higher pressures, as shown in Fig. 21 for Rb, K, and Tl. Instead, the “slow oscillation” behavior seems to dominate the background magnetoresistance behavior. Recent systematic investigations of the temperature-dependent magnetoresistance<sup>62</sup> have also revealed the possibility of a number of new phases in the zero-pressure  $T$ - $H$  plane of the phase diagram. We must therefore consider many aspects of the phase diagram in Fig. 1(a) as provisional.

The mechanism whereby the LTS is destroyed with pressure may be that observed in a number of systems where CDW or SDW states exist. A common example<sup>49</sup> is the Bechgaard salt  $(\text{TMTSF})_2\text{PF}_6$ , which forms a SDW phase below 12 K. Pressures of about 6 kbar remove the SDW in favor of a metallic state (which becomes superconducting below 1 K). For a Peierls-like transition, the electronic energy decreases more than the elastic energy rises, thus driving the transition. However, if by pressure the elastic energy is increased sufficiently, this is no longer the case and the material reverts to the metallic state. Pressure may also induce changes in the shape of the open orbits so that perfect nesting is no longer possible, thereby removing the density-wave state.

Other features associated with the LTS also disappear above  $P_c$ . These include the giant magnetoresistance [see Fig. 22(a)], the negative dips in the AMRO effect<sup>46,47</sup> and the anomalous large second harmonic in the SdH wave form. Our present understanding of the LTS is that the anomalous behavior of the magnetoresistance arises from the reconstructed FS topology shown in Fig. 3(a). Since pressure removes this topology, all associated magneto-transport phenomena also disappear. We note that in

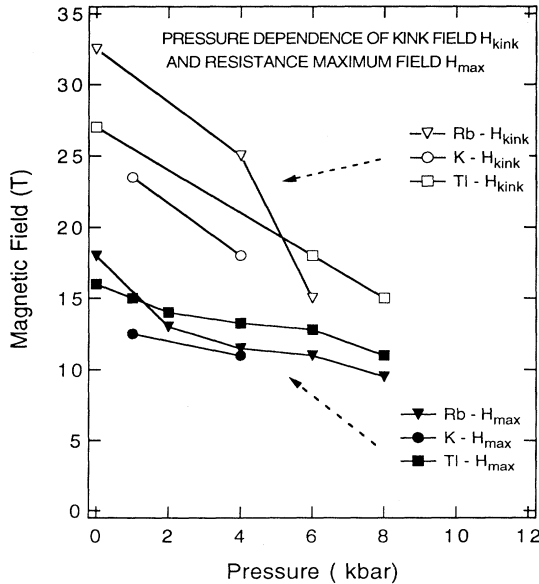


FIG. 21. Pressure dependence of the kink field  $H_{\text{kink}}$  and maximum magnetoresistance field  $H_{\text{max}}$ . It is not possible to follow these features in the magnetoresistance or SdH data above about 8 kbar.

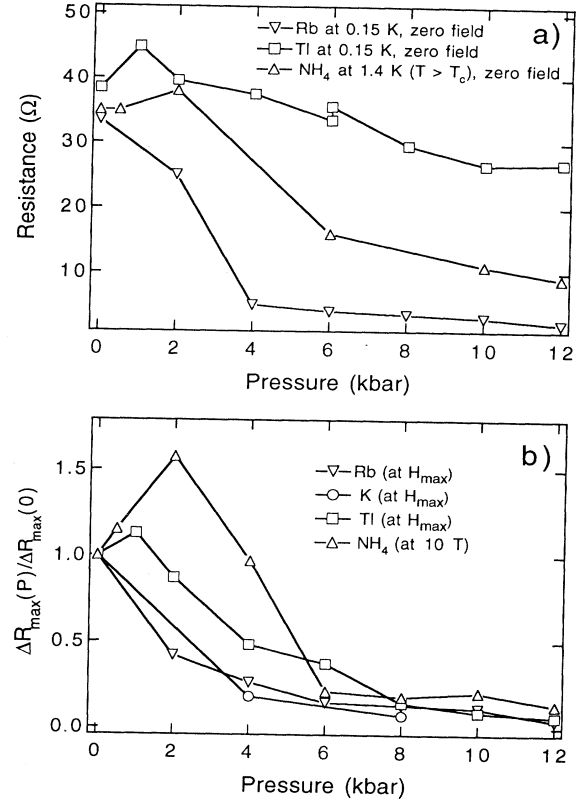


FIG. 22. Pressure dependence of (a) the zero field resistance for  $M=\text{NH}_4$  (for  $T > T_c$ ), Rb, and Tl; and (b) the magnetoresistance change at 10 T for  $M=\text{NH}_4$  and at  $H_{\text{kink}}$  for  $M=\text{K}$ , Rb, and Tl.

some cases the pressure dependence of the second harmonic amplitude at low temperatures actually increases before it decreases. Uneven stress at very low pressures may compromise the density-wave state, whereas slightly higher pressures may better stabilize the transmitting fluid (and the DW state) when it solidifies. Ultimately pressure always destroys the LTS, however.

#### E. Pressure effects on the resistance and magnetoresistance

Hydrostatic pressure is expected to increase the overlap integrals, and lower resistance is expected with increasing pressure. Our results indicate that this process “hardens” above 6 kbar. This trend is true for both the zero-field resistance and for the maximum magnetoresistance at is shown in Fig. 22. At zero field the change in the resistance for  $M=\text{NH}_4$  (for  $T > T_c$ ) is comparable to the other materials. Likewise, even though  $M=\text{NH}_4$  as no density-wave state, its fractional change in magnetoresistance (at 10 T) with pressure is comparable to the others.

### F. Pressure effects on the superconductivity in $\alpha$ -(BEDT-TTF)<sub>2</sub>NH<sub>4</sub>Hg(SCN)<sub>4</sub>

We close this section with a discussion of NH<sub>4</sub>. Much of the work on NH<sub>4</sub> has been previously reported,<sup>56,40</sup> so we will focus only on the pressure dependence of the transition temperature and the effective mass. Two important observations are to be made: (1) The pressure dependence of  $T_c$  is large, and (2) the effective mass decreases rapidly with pressure to the value observed in the density-wave materials ( $\approx 1.5m_0$ ). A consideration of  $dT_c/dP$  leads to new information about the BCS interaction term  $V_{\text{BCS}}$ .

We recall the expression for  $dT_c/dP$  from Sec. III. For  $dT_c/dP \approx -0.25$  K/bar, and  $\beta \approx 1 \times 10^{-2}$ /kbar, we get a value of about 25 for  $1/\beta T_c dT_c/dP$ . For a Debye temperature  $\Theta_D \approx 200$  K, the factor  $1/N(0)V_{\text{BCS}}$  is of order 5, and when multiplied by the term  $d \log N(0)/d \log V$  gives a contribution of order 10. By applying these estimates to the expression for  $dT_c/dP$ , we may rearrange it as follows:<sup>16</sup>

$$3 = -\gamma_g/5 + d \log V_{\text{BCS}}/d \log V.$$

Since the first term on the right-hand side ( $-\gamma_g/5$ ), which involves the Grüneisen constant, is negative and small, this suggests a significant pressure dependence of the remaining BCS interaction term  $d \log V_{\text{BCS}}/d \log V$  in the above expression. Equivalently, the above analysis shows that the effects of pressure on the elastic properties and on the tight-binding parameters cannot account for the large change in  $T_c$  with pressure. Rather, it appears that the  $V_{\text{BCS}}$  interaction term is very sensitive to applied pressure, and this dependence contributes to the destruction of superconductivity in NH<sub>4</sub>.

The above analysis is independent of the effective mass term, and cannot discriminate between the individual contributions to the interaction term. The relation of  $T_c$  and  $m^*$  as modified by pressure are shown in Fig. 23 for both NH<sub>4</sub> and the 10.4-K superconductor  $\kappa$ -(BEDT-TTF)<sub>2</sub>Cu(NCS)<sub>2</sub>. The various possible contributions to the interaction term (electron-phonon and electron-electron) in the organic superconductor  $\kappa$ -(BEDT-TTF)<sub>2</sub>Cu(NCS)<sub>2</sub> based on pressure-dependent and cyclotron resonance studies have been investigated systematically.<sup>41,51</sup> It is possible that although  $T_c$  is an order of magnitude less in  $M=\text{NH}_4$ , the mechanism governing the interaction term is similar in both materials, as the trend in Fig. 23 suggests. A more systematic study along the lines of Refs. 41 and 51 would be very useful to sort out the various terms that contribute to the interaction term for  $M=\text{NH}_4$ .

## VII. CONCLUSIONS

We have used magnetoresistance and the Shubnikov-de Haas effect to probe the effects of pressure on the physical properties of the title materials. These materials have a combination of closed- and open-orbit regions in their Fermi-surface topology. The pressure effects are driven mainly by the anisotropic pressure

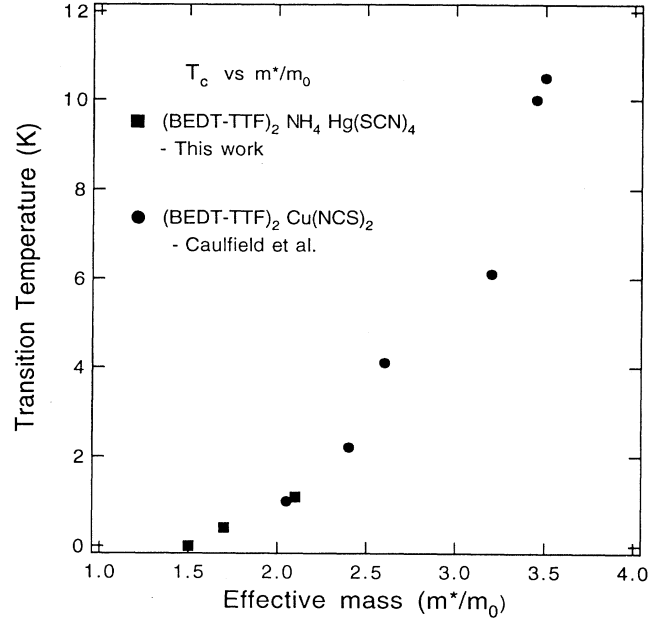


FIG. 23. Superconducting transition temperature vs effective mass for  $\alpha$ -(BEDT-TTF)<sub>2</sub>NH<sub>4</sub>Hg(SCN)<sub>4</sub> and  $\kappa$ -(BEDT-TTF)<sub>2</sub>Cu(NCS)<sub>2</sub> (after Ref. 41).

dependence of the transfer energies, coupled with a high degree of compressibility. We have discovered that the pressure effects on the band structure are more complex than the simple expansion of the BZ with decreasing lattice constant. We have found that for the superconductor studied,  $T_c$  and  $m^*$  are highly pressure dependent, and we argue that it is the pressure dependence of the BCS interaction that influences this behavior. Furthermore, for those materials with density-wave ground state, pressure removes the density-wave state above a critical pressure  $P_c$ . Finally, pressure induces new features in the Fermi surface—a mechanism that most likely involves new nesting conditions involving the open orbits.

High-pressure studies of these materials holds great promise for future work. The materials are high-purity single crystals, with many manifestations of low-dimensional physical mechanisms. Indeed the charge transfer between the conducting and nonconducting planes is very similar to the concept of modulation doping used in the GaAs/Al<sub>x</sub>Ga<sub>1-x</sub>As heterostructures where carriers are introduced into ultrahigh purity material without the direct introduction of impurities. In the case of the title materials, the carrier concentration cannot be changed by doping due to the nature of the charge transfer. However, due to the highly compressible nature of the materials, the electronic structure can be easily altered, and new Fermi-surface topologies realized. Even at extreme pressures of up to 50 kbar, the high-quality single-crystal nature of the samples remains, but the changes in the electronic structure may be equal to or greater than the original bandwidth. Hence these materi-

als may be driven with pressure into entirely new configurations of matter. The present work indicates that orbits, very near the quantum limit at 20 T, have been stabilized by pressure. Hence pressure may provide a way to move the materials into a regime where such effects as the quantum Hall effect in a bulk quasi-two-dimensional material may be observable. Angular-dependent magnetoresistance studies at high pressures will be useful to determine in more detail the altered Fermi-surface topology. Diamond anvil studies should produce electronic configurations at very high pressures (up to 100 kbar). Pressure-dependent band-structure and Fermi-surface calculations are in progress<sup>50</sup> to follow computationally the electronic configurations that are induced by pressure.

## ACKNOWLEDGMENTS

Research at Boston University is supported by NSF DMR 92-14889. The authors are indebted to the staff of the F. B. National Magnet Laboratory and to the National High Magnetic Field Laboratory (both supported by the National Science Foundation) where much of this work was carried out. We are particularly thankful to P. Emery of the FBNML, and to P. Henning, P. Kuhns, and E. Palm of the NHMFL for their help during many stages of this work. The authors also thank Dr. S. Uji and Dr. H. Aoki for important discussions.

\*Present address: Physics Department, Florida State University, 1800 E. Paul Dirac Drive, Tallahassee, FL 32306-4005.

<sup>†</sup>Present address: Electrical Engineering Department, University of California, Santa Barbara, CA 93106.

<sup>1</sup>H. Mori, S. Tanaka, K. Oshima, G. Saito, T. Mori, Y. Maruyama, and H. Inokuchi, *Synth. Met.* **42**, 2013 (1991).

<sup>2</sup>H. Mori, S. Tanaka, M. Oshima, G. Saito, T. Mori, M. Maruyama, and H. Inokuchi, *Bull. Chem. Soc. Jpn.* **63**, 2183 (1990).

<sup>3</sup>N. D. Kushch, L. I. Buravov, M. V. Kartsovnik, V. N. Laukhin, S. I. Petrovskii, R. P. Shibaeva, L. P. Rosenberg, E. B. Yagubskii, and A. V. Zvarykina, *Synth. Met.* **46**, 2761 (1992).

<sup>4</sup>H. H. Wang, K. D. Carlson, U. Geiser, W. K. Kwok, M. D. Vashon, J. E. Thompson, N. F. Larsen, G. D. McCabe, R. S. Hulscher, and J. M. Williams, *Physica (Amsterdam) C* **166**, 57 (1990).

<sup>5</sup>Various aspects of organic conductor physics have been reported at two recent international conferences: Proceedings of the 4th International Symposium on Research in High Magnetic fields, Nijmegen, 1994, edited by J. A. A. G. Perenboom [*Physica B* **1-4**, (1995)] and Proceedings of the International Conference on the Science and Technology of Synthetic Metals, Seoul, 1994, edited by A. J. Heeger [*Synth. Met.* **1-3** (1995)].

<sup>6</sup>T. Mori, A. Kobayashi, Y. Sasaki, H. Kobayashi, G. Saito, and H. Inokuchi, *Bull. Chem. Soc. Jpn.* **57**, 627 (1984).

<sup>7</sup>L. Ducasse and A. Fritsch, *Solid State Commun.* **91**, 201 (1994).

<sup>8</sup>D. Shoenberg, *Magnetic Oscillations in Metals* (Cambridge University Press, Cambridge, 1994).

<sup>9</sup>Y. Iye, R. Yagi, N. Hanasaki, S. Kagoshima, H. Mori, H. Fujimoto, and G. Saito (unpublished).

<sup>10</sup>We find that especially in magnetic fields above 30 T the SdH wave forms become highly nonsinusoidal, and the Lifshitz-Kosevich formalism does not yield the effective mass directly. P. Sandhu *et al.* (unpublished).

<sup>11</sup>V. N. Laukhin, A. Audouard, H. Rakoto, J. M. Broto, F. Goze, G. Coffe, L. Brossard, J. P. Redoules, M. V. Kartsovnik, N. D. Kushch, L. I. Buravov, A. G. Khomenko, E. B. Yagubski, S. Askenazy, and P. Pari, *Physica (Amsterdam)* **211B**, 282 (1995).

<sup>12</sup>F. Pratt, T. Sasaki, N. Toyota, and K. Nagamine, *Phys. Rev. Lett.* **74**, 3892 (1995).

<sup>13</sup>K. Kanoda, A. Kawamoto, K. Niyagawa, and Y. Nakazawa,

*Synth. Met.* **70**, 973 (1995).

<sup>14</sup>T. Sasaki and N. Toyota, *Solid State Commun.* **82**, 447 (1992).

<sup>15</sup>J. S. Brooks, C. C. Agosta, S. J. Klepper, M. Tokumoto, N. Kinoshita, H. Anzai, S. Uji, H. Aoki, A. S. Perel, G. J. Athas, and D. A. Howe, *Phys. Rev. Lett.* **69**, 156 (1992).

<sup>16</sup>X. Chen, Ph.D. thesis, Boston University, 1994 (this paper is based in part on this thesis work).

<sup>17</sup>A. I. Schegolev, V. N. Laukhin, A. G. Khomenko, M. V. Kartsovnik, R. P. Shibaeva, L. P. Rozenberg, and A. E. Kovalev, *J. Phys. (France) I* **2**, 2123 (1992).

<sup>18</sup>T. Sasaki, N. Toyota, M. Tokumoto, N. Kinoshita, and H. Anzai, *Solid State Commun.* **75**, 93 (1990).

<sup>19</sup>T. Sasaki, T. Toyota, M. Tokumoto, N. Kinoshita, and H. Anzai, *Solid State Commun.* **75**, 93 (1990).

<sup>20</sup>N. Kinoshita, M. Tokumoto, and H. Anzai, *J. Phys. Soc. Jpn.* **59**, 3410 (1990).

<sup>21</sup>T. Sasaki, N. Toyota, M. Tokumoto, N. Kinoshita, and H. Anzai, *Solid State Commun.* **75**, 97 (1990).

<sup>22</sup>H. Mori, I. Hirabayashi, S. Tanaka, T. Mori, H. Inokuchi, K. Oshima, and G. Saito, *Synth. Met.* **55-57**, 2443 (1993).

<sup>23</sup>N. Kinoshita, M. Tokumoto, and H. Anzai, *J. Phys. Soc. Jpn.* **60**, 2131 (1991).

<sup>24</sup>T. Osada, R. Yagi, A. Kawasumi, S. Kagoshima, N. Miura, M. Oshima, and G. Saito, *Phys. Rev. B* **41**, 5428 (1990).

<sup>25</sup>M. B. Kartsovnik, D. V. Mashovets, D. V. Smirnov, V. N. Laukhin, A. Gilewski, and N. D. Kushch, *J. Phys. (France) I* **4**, 159 (1994).

<sup>26</sup>G. J. Athas, S. J. Klepper, J. S. Brooks, M. Tokumoto, T. Kinoshita, N. Kinoshita, and H. Anzai, *Synth. Met.* **70**, 843 (1995).

<sup>27</sup>J. S. Brooks, S. J. Klepper, C. C. Agosta, M. Tokumoto, N. Kinoshita, Y. Tanaka, S. Uji, H. Aoki, G. J. Athas, X. Chen, and H. Anzai, *Synth. Met.* **55-57**, 1791 (1993).

<sup>28</sup>T. Sasaki and N. Toyota, *Phys. Rev. B* **48**, 11457 (1993), and references therein.

<sup>29</sup>S. Uji, H. Aoki, M. Tokumoto, N. Kinoshita, H. Anzai, J. S. Brooks, A. S. Perel, G. J. Athas, S. J. Klepper, C. C. Agosta, and D. A. Howe, in *Highly Correlated, Low Dimensional Electron Systems in Organic Conductors*, edited by N. Toyota (Tohoku University, Sendai, 1992), p. 6.

<sup>30</sup>J. Caulfield, S. J. Blundell, M. S. L. du Croo de Jongh, P. T. J. Hendriks, J. Singleton, M. D'Orto, F. L. Pratt, A. House, J. A. A. J. Perenboom, W. Hayes, M. Kurmoo, and P. Day, *Phys. Rev. B* **51**, 8325 (1995).

- <sup>31</sup>G. J. Athas, J. S. Brooks, S. Valfells, S. J. Klepper, M. Tokumoto, N. Kinoshita, T. Kinoshita, and Y. Tanaka, *Phys. Rev. B* **50**, 17 713 (1994).
- <sup>32</sup>K. Yamaji, *J. Phys. Soc. Jpn.* **58**, 1520 (1989); R. Yagi, Y. Iye, T. Osada, and S. Kagoshima, *ibid.* **59**, 3069 (1990).
- <sup>33</sup>S. Kagoshima, T. Osada, A. Kawasumi, R. Yagi, N. Miura, M. Oshima, H. Mori, T. Nakamura, and G. Saito, in *Mechanics of Superconductivity* [special issue of *Jpn. J. Appl. Phys.* **7**, 381 (1992)].
- <sup>34</sup>J. Caulfield, J. Singleton, P. T. J. Hendriks, J. A. A. J. Perenboom, F. L. Pratt, M. Doporto, W. Hayes, M. Kurmoo, P. Day, *J. Phys. Condens. Matter* **6**, L155 (1994); P. Hendriks, D.D. thesis, University of Nijmegen, 1993.
- <sup>35</sup>G. J. Athas, S. J. Klepper, J. S. Brooks, M. Tokumoto, N. Kinoshita, and Y. Tanaka, *Physica (Amsterdam)* **194-196B**, 2003 (1994).
- <sup>36</sup>M. V. Kartsovnik, A. E. Kovalev, and N. D. Kushch, *J. Phys. (France) I* **3**, 1187 (1993), and references therein.
- <sup>37</sup>S. Uji, H. Aoki, J. S. Brooks, A. S. Perel, G. J. Athas, S. J. Klepper, C. C. Agosta, D. A. Howe, M. Tokumoto, T. Kinoshita, N. Kinoshita, Y. Tanaka, and H. Anzai, *Solid State Commun.* **88**, 683 (1993).
- <sup>38</sup>S. Uji, T. Terashima, H. Aoki, J. S. Brooks, M. Tokumoto, N. Kinoshita, T. Kinoshita, Y. Tanaka, and H. Anzai, *J. Phys. Condens. Matter* **6**, L539 (1994).
- <sup>39</sup>J. S. Brooks, G. J. Athas, S. J. Klepper, X. Chen, C. E. Campos, S. Valfells, Y. Tanaka, T. Kinoshita, N. Kinoshita, M. Tokumoto, and H. Anzai, *Physica B (Amsterdam)* **201**, 449 (1994).
- <sup>40</sup>J. S. Brooks, S. Uji, H. Aoki, T. Terashima, M. Tokumoto, N. Kinoshita, Y. Tanaka, and H. Anzai, *Synth. Met.* **70**, 839 (1995).
- <sup>41</sup>J. Caulfield, W. Lubczynski, F. L. Pratt, J. Singleton, D. Y. K. Ko, W. Hayes, M. Kurmoo, and P. Day, *J. Phys. Condens. Matter* **6**, 2911 (1994).
- <sup>42</sup>H. Ito, H. Kaneko, and T. Ishiguro, *Solid State Commun.* **85**, 1005 (1993).
- <sup>43</sup>H. Ito, M. V. Kartsovnik, H. Ishimoto, K. Kono, H. Mori, N. D. Kushch, G. Saito, T. Ishiguro, and S. Tanaka, *Synth. Met.* **70**, 899 (1995).
- <sup>44</sup>J. S. Brooks, S. J. Klepper, X. Chen, P. Henning, P. J. C. Signore, M. W. Meisel, N. Kinoshita, M. Tokumoto, and H. Anzai, *Appl. Supercond.* **2**, 759 (1995).
- <sup>45</sup>R. Kuono, T. Osada, M. Hasumi, S. Kagoshima, N. Miura, M. Oshima, H. Mori, T. Nakamura, and G. Saito, *Synth. Met.* **55-57**, 2425 (1993).
- <sup>46</sup>S. Kagoshima, in *Highly Correlated, Low Dimensional Electron Systems in Organic Conductors* (Ref. 29), p. 10.
- <sup>47</sup>M. V. Kartsovnik, A. E. Kovalev, V. N. Laukhin, I. F. Schegolev, H. Ito, T. Ishiguro, N. D. Kushch, H. Mori, and G. Saito, *Synth. Met.* **70**, 811 (1995).
- <sup>48</sup>D. Chasseau, J. Gaultier, M. Rahal, L. Ducasse, M. Kurmoo, and P. Day, *Synth. Met.* **41-43**, 2039 (1991).
- <sup>49</sup>See, for example, T. Ishiguro and K. Yamaji, *Organic Superconductors* (Springer-Verlag, Berlin, 1990).
- <sup>50</sup>We have recently investigated the pressure dependence of the transfer energies and find, for example, that the  $C$  and  $p$  terms in Fig. 2(b) do not scale in the same way with a uniform change in the lattice parameters; P. Sandhu, C. E. Campos, and J. S. Brooks (unpublished).
- <sup>51</sup>S. O. Hill, J. Singleton, F. L. Pratt, M. Doporto, W. Hayes, T. J. B. M. Janseen, J. A. A. J. Perenboom, M. Kurmoo, and P. Day, *Synth. Met.* **55-57**, 2566 (1993).
- <sup>52</sup>X. Chen, A. S. Perel, J. S. Brooks, R. P. Guertin, and D. G. Hinks, *J. Appl. Phys.* **73**, 1886 (1993).
- <sup>53</sup>J. D. Thompson, *Rev. Sci. Instrum.* **55**, 231 (1984).
- <sup>54</sup>Recently, it has been reported that uniaxial stress induces superconductivity for  $M=K$ , and increases  $T_c$  for  $M=NH_4$ . C. E. Campos, J. S. Brooks, P. J. M. van Bentum, J. A. A. J. Perenboom, S. J. Klepper, P. Sandhu, S. Valfells, Y. Tanaka, T. Kinoshita, N. Kinoshita, M. Tokumoto, and H. Anzai, *Phys. Rev. B* **52**, 7014 (1995).
- <sup>55</sup>G. J. Athas, S. J. Klepper, J. S. Brooks, M. Tokumoto, T. Kinoshita, N. Kinoshita, and H. Anzai, *Synth. Met.* **70**, 843 (1995).
- <sup>56</sup>S. J. Klepper, J. S. Brooks, X. Chen, I. Bradaric, M. Tokumoto, N. Kinoshita, Y. Tanaka, and C. C. Agosta, *Phys. Rev. B* **48**, 9913 (1993). We note that the effective mass  $m^*=(1.4\pm 0.2)m_0$  quoted in this paper was the average of the high-pressure data, and did not include the zero-pressure value, which is significantly larger. In Ref. 10 a value  $m^*=2.6m_0$  is found at the lowest (pulsed) field of 16 T at zero pressure. A similar result was reported in steady-state fields by J. Wosnitza, G. W. Crabtree, H. H. Wang, U. Geiser, J. M. Williams, and K. D. Carlson, *Phys. Rev. B* **45**, 3018 (1992).
- <sup>57</sup>R. H. McKenzie, J. S. Brooks, R. G. Clark, R. Newbury, R. P. Starrett, A. Skougarevsky, R. A. Lewis, S. Takasaki, J. Yamada, H. Anzai, Y. Tanaka, T. Kinoshita, N. Kinoshita, M. Tokumoto, and M. Kartsovnik (unpublished).
- <sup>58</sup>S. Valfells, J. S. Brooks, W. W. Tozer, S. J. Klepper, Y. Tanaka, T. Kinoshita, N. Kinoshita, M. Tokumoto, and H. Anzai, *Solid State Commun.* **94**, 499 (1995).
- <sup>59</sup>A. E. Kovalev, M. V. Kartsovnik, R. P. Shibaeva, L. P. Rozenberg, and I. F. Schegolev, *Solid State Commun.* **89**, 575 (1994).
- <sup>60</sup>P. Auban-Senzier, A. Audouard, V. N. Laukhin, R. Rousseau, E. Canadell, L. Brossard, D. Jerome, and N. D. Kushch, *J. Phys. (France) I* (to be published).
- <sup>61</sup>C. E. Campos, J. S. Brooks, P. J. M. van Bentum, J. A. A. J. Perenboom, S. J. Klepper, P. Sandhu, M. Tokumoto, T. Kinoshita, N. Kinoshita, Y. Tanaka, and H. Anzai, *Synth. Met.* **70**, 803 (1995).
- <sup>62</sup>T. Sasaki, T. Fukase, and N. Toyota (unpublished).

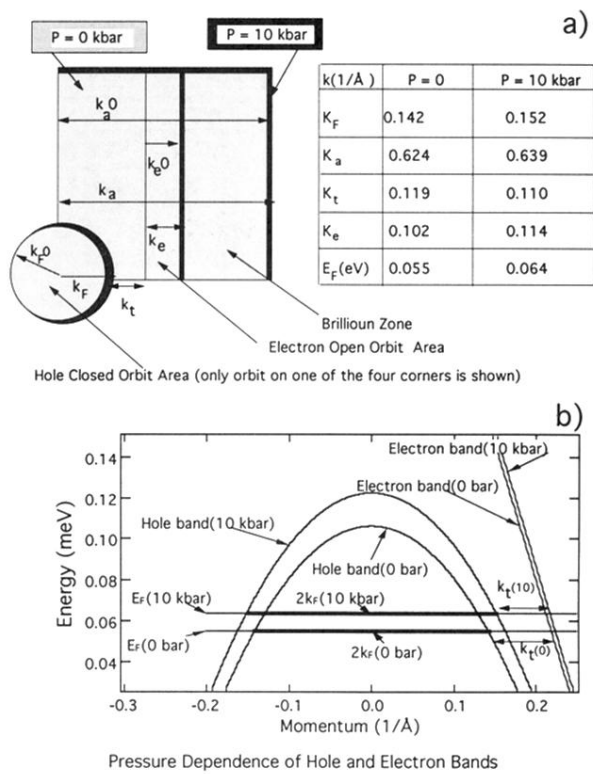


FIG. 19. Pressure dependence of Fermi surface and band structure in  $\alpha$ -(BEDT-TTF) $_2$ MHg(SCN) $_4$ . (a) Description of the main Fermi surface features at 0 and 10 kbar. (b) Behavior of hole and electron bands near the Fermi level.

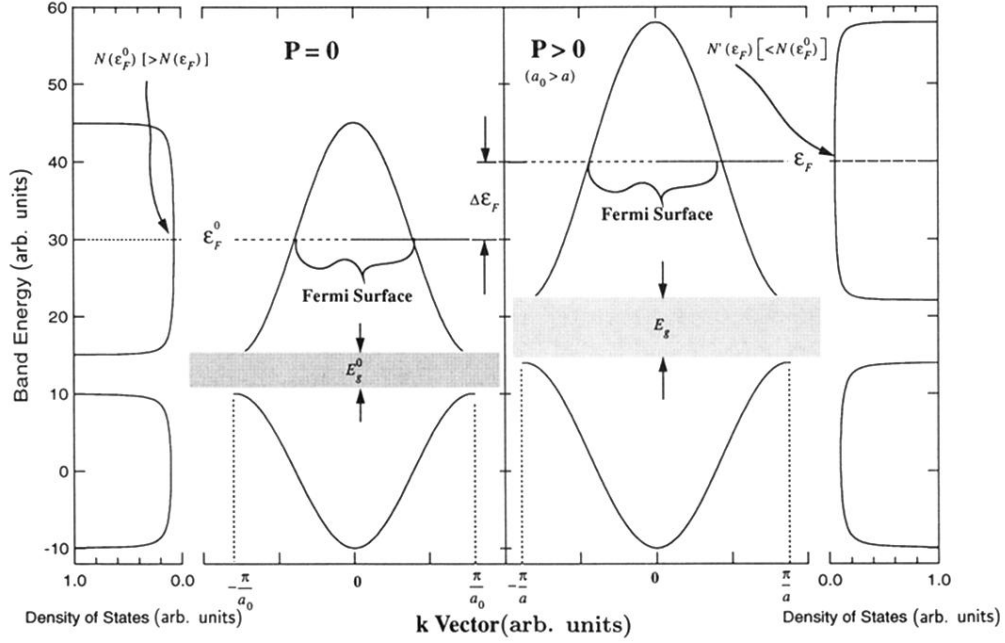


FIG. 6. Schematic pressure dependence of the tight-binding energy band, the Fermi level, and the density of states. On the left, we show the configuration at ambient pressure with lattice constant  $a_0$ , Fermi level  $\epsilon_F^0$ , and band gap  $E_g^0$ . The intersection of the Fermi level and the hole band forms the Fermi surface. On the right, we show the changes that result from a decrease in the lattice constant to  $a$  for increasing pressure: (i) The energy band expands in  $k$  space as the first BZ expands. (ii) The bandwidth increases in energy. (iii) While maintaining the filling of the band, the Fermi level increases by  $\Delta\epsilon_F$ . (iv) The band gap increases to  $E_g$ . (v) The density of states function  $N(\epsilon)$  changes into  $N'(\epsilon)$  (i.e., the density of states at the Fermi level decreases). (vi) The intersection of the band with the Fermi surface increases, which, if extended to two dimensions, means that the associated hole orbit area increases with pressure.